Journal Pre-proofs

Research Article

Insights into Ligand-Mediated Activation of an Oligomeric Ring-Shaped Gene-Regulatory Protein from Solution- and Solid-State NMR

Rodrigo Muzquiz, Cameron Jamshidi, Daniel W. Conroy, Christopher P. Jaroniec, Mark P. Foster

PII: S0022-2836(24)00414-5

DOI: https://doi.org/10.1016/j.jmb.2024.168792

Reference: YJMBI 168792

To appear in: Journal of Molecular Biology

Received Date: 11 May 2024
Revised Date: 18 August 2024
Accepted Date: 9 September 2024



Please cite this article as: R. Muzquiz, C. Jamshidi, D.W. Conroy, C.P. Jaroniec, M.P. Foster, Insights into Ligand-Mediated Activation of an Oligomeric Ring-Shaped Gene-Regulatory Protein from Solution- and Solid-State NMR, *Journal of Molecular Biology* (2024), doi: https://doi.org/10.1016/j.jmb.2024.168792

This is a PDF file of an article that has undergone enhancements after acceptance, such as the addition of a cover page and metadata, and formatting for readability, but it is not yet the definitive version of record. This version will undergo additional copyediting, typesetting and review before it is published in its final form, but we are providing this version to give early visibility of the article. Please note that, during the production process, errors may be discovered which could affect the content, and all legal disclaimers that apply to the journal pertain.

© 2024 Elsevier Ltd. All rights are reserved, including those for text and data mining, AI training, and similar technologies.

Insights into Ligand-Mediated Activation of an Oligomeric Ring-Shaped Gene-Regulatory Protein from Solution- and Solid-State NMR

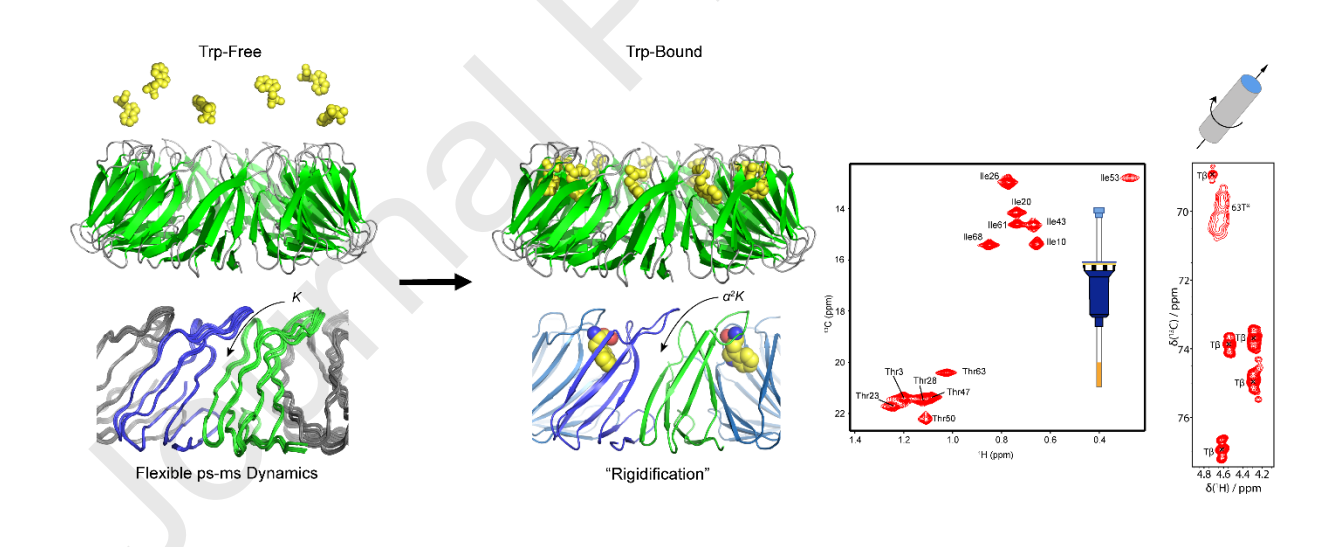
Rodrigo Muzquiz^{a,b}, Cameron Jamshidi^{a,b}, Daniel W. Conroy^b, Christopher P. Jaroniec^{a,b}, and Mark P. Foster^{a,b,*}

^a Ohio State Biochemistry Graduate Program, The Ohio State University, 484 West 12th Avenue, Columbus, OH 43210, USA

^b Department of Chemistry and Biochemistry, The Ohio State University, 100 West 18th Avenue, Columbus, OH 43210, USA

*Correspondence to: foster.281@osu.edu; 614-292-1377

Declarations of interest: none



Highlights

Oligomeric ligand-activated protein rings exhibit dynamic allostery

- Methyl-TROSY NMR in solution measures fast and intermediate dynamics
- Dipolar-couplings in solid-state NMR correlate rigid regions
- Scalar couplings in solids-state NMR reveal flexible regions
- Dynamics enable ligand binding and quenching dynamics leads to cooperativity

Abstract

The 91 kDa oligomeric ring-shaped ligand binding protein TRAP (trp RNA binding attenuation protein) regulates the expression of a series of genes involved in tryptophan (Trp) biosynthesis in bacilli. When cellular Trp levels rise, the free amino acid binds to sites buried in the interfaces between each of the 11 (or 12, depending on the species) protomers in the ring. Crystal structures of Trp-bound TRAP show the Trp ligands are sequestered from solvent by a pair of loops from adjacent protomers that bury the bound ligand via polar contacts to several threonine residues. Binding of the Trp ligands occurs cooperatively, such that successive binding events occur with higher apparent affinity but the structural basis for this cooperativity is poorly understood. We used solution methyl-TROSY NMR relaxation experiments focused on threonine and isoleucine sidechains, as well as magic angle spinning solid-state NMR ¹³C-¹³C and ¹⁵N-¹³C chemical shift correlation spectra on uniformly labeled samples recorded at 800 and 1200 MHz, to characterize the structure and dynamics of the protein. Methyl ¹³C relaxation dispersion experiments on ligand-free apo TRAP revealed concerted exchange dynamics on the µs-ms time scale, consistent with transient sampling of conformations that could allow ligand binding. Cross-correlated relaxation experiments revealed widespread disorder on fast timescales. Chemical shifts for methyl-bearing side chains in apo- and Trp-bound TRAP revealed subtle changes in the distribution of sampled sidechain rotameric states. These observations reveal a pathway and mechanism for induced conformational changes to generate homotropic Trp-Trp binding cooperativity.

Keywords

Allostery; ring protein; solid state NMR; dynamics; methyl relaxation dispersion

Abbreviations

TRAP, *trp* RNA-binding attenuation protein; CSP, chemical shift perturbation; CP-MAS, cross-polarization magic-angle spinning; TROSY, transverse relaxation optimized spectroscopy; MQ, multiple-quantum; RD, relaxation dispersion; DQC, double-quantum coherence; SQC, single-quantum coherence; DARR, dipolar-assisted rotational resonance

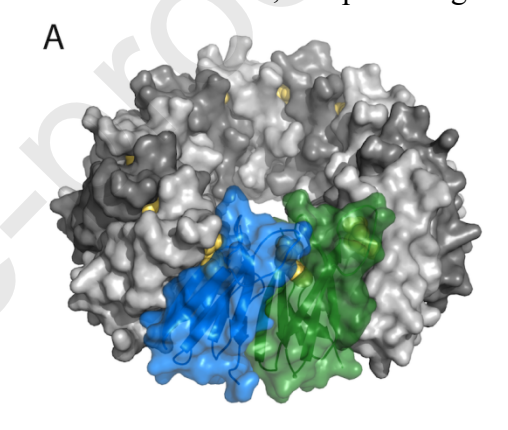
Introduction

Ligand-mediated regulation of protein function involves changes in its functional state that accompany binding of one or more ligands [1–3]. When the ligands bind at sites remote from the site of function, this regulation is referred to as "allosteric" [4,5]. Allosteric regulation is widespread in biology, governing processes ranging from trans-membrane signaling, enzyme activity and gene expression[6–9]. There is considerable interest in understanding the mechanisms of allosteric regulation, as this could provide means of manipulating essential processes, or engineering new desired regulatory systems [4,5,10,11]. NMR spectroscopy has advantages for studying allostery due to is unique ability to provide information on both structure and dynamics at multiple sites, detecting lowly populated conformational states, and providing

site-specific information on conformational entropy [1,12–15]. Of paramount interest is detailing *how* ligand binding at an allosteric site is transmitted through the

protein to sites responsible for its activity.

To gain insights into mechanisms of allosteric regulation we studied the ring-shaped undecameric (11-mer) protein TRAP (trp RNA binding attenuation protein) from Geobacillus stearothermophilus (Figure 1). TRAP is a paradigmatic allosteric protein that regulates expression of the Trp biosynthesis genes at the levels of transcription and translation [16,17]. At high cellular concentrations of tryptophan (Trp) TRAP binds up to eleven Trp ligands and is activated to bind with high affinity to specific sequences in the 5' leader of the trp operon mRNA. This interaction leads to premature transcription termination, and in the full transcript, results in sequestration of the Shine-Dalgarno sequence, inhibiting its translation. At low Trp levels, unbound (apo) TRAP is inactive for RNA binding. Crystal structures of Trp-bound (holo) TRAP reveal that Trp ligands bind between adjacent protomers with the indole ring buried in the hydrophobic pocket formed by β -sheets [18–20]. The Trp ligands bind cooperatively to TRAP. such that successive ligand binding events occur with higher apparent affinity [21,22]. Specificity for Trp arises from a series of polar contacts between each Trp ligand and the BC loop of one protomer and the DE loop of the adjacent protomer [23]. Crystal structures show that the resulting binding pocket entirely secludes Trp from solvent. This suggests that in addition to the observed



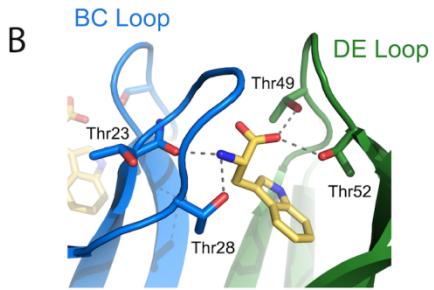


Figure 1: Homo-undecameric TRAP rings bury up to eleven Trp ligands in the interface between adjacent protomers.
(A) Undecameric TRAP ring as observed in Trp-bound crystals (PDB:1C9S) shows the ligands are completely excluded from solvent. One protomer is blue, one green, and the others are grey.
(B) Four threonine residues from the BC and DE loops contact the carboxyl and amino groups of the buried Trp ligands

Trp-bound state the protein must sample alternative conformations that allow Trp to bind to and dissociate from its sites in the protein-protein interfaces.

Prior solution NMR studies of the 90.6 kDa TRAP oligomer have shown that in the absence of Trp a high degree of conformational flexibility in the ligand binding loops results in extreme line broadening of backbone amide resonances [24–26]. This flexibility presents obstacles to detailed structural analysis of apo TRAP by both crystallography and solution NMR; that is, the parts of the protein that are of most interest are also the most difficult to observe. The large molecular weight of the protein rings also presents a challenge to solution NMR as their slow molecular tumbling results in fast transverse relaxation, broad signals and decreased intensity in spectra. Despite these limitations, the use of TROSY-based NMR methods along with increased temperature and uniform deuteration enabled backbone resonance assignments of a most of the residues in holo TRAP and 39 residues in apo TRAP; notably, most of the residues in the BC and DE loops could be assigned in holo TRAP but are absent in spectra of apo TRAP [24]. Labeling of the methyl groups of Ile, Leu and Val sidechains enabled more detailed characterization of the effect of ligand binding on the structure and dynamics of the protein, although those residues are not present in the BC and DE loops of the native protein[25]. These spectral differences between apo and holo TRAP reveal that the ligand profoundly rigidifies the ligand binding site, with more modest effects on residues in the structured of the protein ring [24,25]. Nevertheless, the absence in apo TRAP spectra of signals from the Trp-binding BC and DE loops limits the conclusions that can be drawn about the mechanism of Trp access to its sites, or the basis for Trp-Trp cooperativity.

Here we advance our understanding of the structure and dynamics of apo TRAP by application of complementary solution and solid-state NMR approaches. Introduction of threonine methyl labeling has enabled more direct characterization of the structure and dynamics of the BC and DE loops. Moreover, the limitations associated with molecular tumbling and intermediate exchange broadening can in principle be alleviated by the use of magic angle spinning (MAS) solid-state NMR, a robust spectroscopic tool that is not inherently limited by molecular size [27–29]. Specifically, multidimensional solid-state NMR techniques that rely on polarization transfers based on dipolar and J-couplings can facilitate detailed characterization of structure and conformational dynamics for relatively rigid and highly flexible protein domains, respectively, and have been successfully employed to probe a range of high-molecular weight protein complexes and assemblies including membrane proteins, amyloids, supramolecular machines, viral protein assemblies, and chromatin [30–33]. By combining solution NMR spin-relaxation measurements at 600 and 800 MHz, and MAS solid-state NMR at 800 at 1200 MHz, we quantify the loop dynamics in TRAP that gate access by Trp to its binding sites and illuminate the shifts in the free energy landscape that result in cooperative ligand binding.

Results

Threonine Methyl Resonance Assignments

We prepared samples of A26I-TRAP in which the δ_1 -methyl carbons of Ile, and γ_2 -methyl carbons of Thr were labeled with ¹³C, while other carbon-bound protons were deuterated and all

nitrogen positions enriched with ¹⁵N; i.e., Thr/Ile-[¹³CH₃], U-[²H,¹⁵N]-A26I-TRAP. The mutation of Ala26 to Ile was previously engineered to introduce an additional Ile methyl probe in the BC loop of the protein, and to serve as a metric of Trp binding [25]. Trp and RNA binding experiments, and NMR spectra showed that the A26I mutation did not significantly perturb TRAP structure or function. Although the Thr residues labeled here serve as native monitor probes of the loops, the A26I mutation was retained for consistency with those prior experiments [25].

Thr side chain methyl resonances of TRAP were assigned from a combination of through-space NOE correlations in solution at 55 °C, and through-bond correlations in solid-state NMR spectra.

Prior studies had assigned the methyl resonances of Ile, Val and Leu (ILV) residues using a series of solution triple-resonance and "out-and-back" methyl correlation experiments[25]. While those resonances provided useful probes of the structure and dynamics of the apo and holo states of the protein, the absence of native ILV residues in the BC and DE loops left their dynamics poorly understood. In this study Thr methyl signals in apo-TRAP were assigned using 3D CCH HMOC-NOESY-HMOC and ¹³C-edited NOESY-HMQC (HCH) spectra[34]. Five of the six Thr methyls could be assigned based on strong NOEs to proximal Ile methyl groups referencing the crystal structure of Trp-bound TRAP (Table S 1). For example, the Thr50 γ-methyl is within NOE-distance to both Ile53 and Ile26 delta-methyl and shows a cross peak in both the HCH and CCH NOESY spectra (Figure 2, Table S 1). Thr3, present in the disordered N-terminus of the protein was assigned by process of elimination[24].

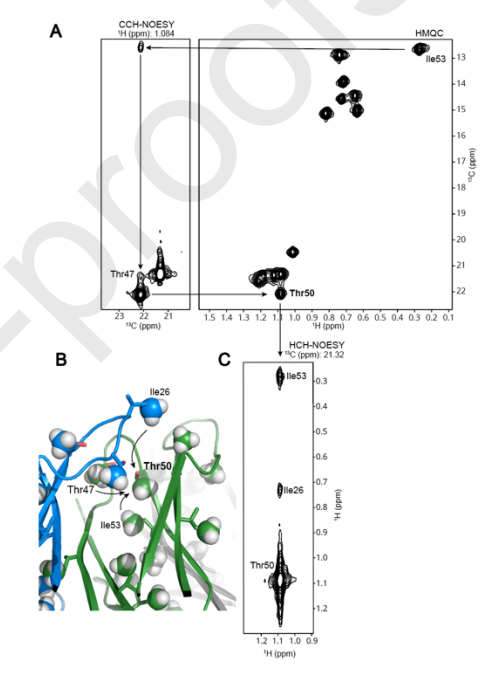


Figure 2. Assignment of Thr γ_2 methyl resonances of apo TRAP from 13 C- and 1 H-separated NOESY spectra, at 55° C. (A) Right, methyl TROSY spectrum; left, CCH-NOESY plane corresponding to the Thr50 γ_2 methyl 1 H resonance. (B) Model from the Trp-TRAP crystal structure, illustrating NOEs observed to Thr50. (C) Plane from 13 C-separated NOESY-HMQC spectrum corresponding to the Thr50 γ_2 13 C methyl resonance.

Methyl-TROSY NMR Spectra Reveal Trp-Induced Structural Perturbations

To monitor Trp-induced conformational changes in TRAP, we acquired 2D ¹H-¹³C-correlated methyl TROSY-HMOC spectra of A26I-TRAP in its Trp-free apo and Trp-bound holo states (Figure 3A). Axial symmetry of TRAP in these states is evident from the observation of a single set of signals in the ¹H-¹³C methyl spectra. The benefits of the methyl TROSY effect are evident in the spectra of the 90.6 kDa apo protein as we observe seven Ile (including the extra signal from the A26I mutation) and six Thr methyl signals that have uniform intensities. The ¹³C shifts of four Thr are highly

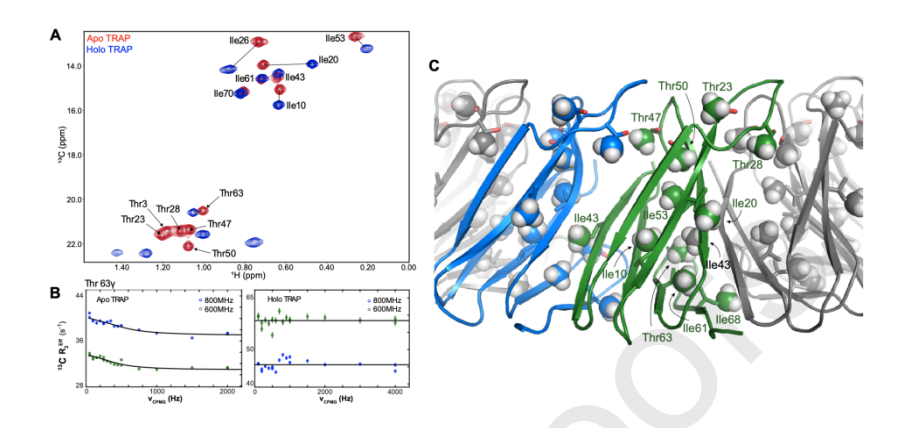


Figure 3: Trp binding alters the structure and dynamics of TRAP rings. (A) 1 H- 13 C methyl TROSY-HMQC spectra of $[U-^{2}H/^{15}N, Thr/Ile-^{1}H/^{13}C$ -methyl]-A26I-TRAP recorded at 800 MHz, 55 °C in the absence (apo, red) and presence (holo, blue) of Trp. Most Thr and Ile methyl resonances are strongly perturbed by Trp binding. (B) Multiple quantum 13 C relaxation dispersion (MQ RD) profiles for the Thr63 methyl group recorded at 800 (blue) and 600 (green) MHz at 20 °C in the absence (left) and presence (right) of Trp. Large dispersions observed in spectra of apo TRAP are not observed in spectra of holo TRAP. Lines are fits of the frequency dependence of the effective transverse relaxation rate with a site-specific two-state exchange model for apo TRAP and no exchange for holo TRAP. R_2^{eff} two a site-specific two-state exchange model for apo TRAP and no exchange for holo TRAP.

degenerate in apo TRAP (Figure 3A), with four of the six near 21.5 ppm, suggestive of similar time- and ensemble-averaged conformations. In the Trp-bound holo form we observe increased dispersion in the ¹³C dimension as well as variable intensities for the Thr methyl signals, with the sixth signal not observable at 55 °C. Comparing the apo and holo spectra we observed increased chemical shift dispersion for all Thr methyl groups even though only four are proximal to the Trp binding site in the crystal structure of Trp-bound TRAP (Figure 1)[35]. This indicates that structural consequences of ligand binding are not restricted to the immediacy of the Trp binding site, implicating allosteric structural changes.

CPMG NMR Relaxation Dispersion Reveals Complex Exchange Dynamics

Availability of methyl resonance assignments enabled site-specific interpretation of methyl NMR relaxation dispersion (RD) experiments performed on apo TRAP. RD experiments were performed at 20 °C instead of 55 °C with the expectation that this might result in slow exchange for some of the methyl resonances; methyl spectra at 20 °C were of comparable quality (Figure S 5). These experiments revealed dynamics on the μ s-ms time scale in the Trp-gating BC and DE loops in apo A26I-TRAP. Multiple-quantum (MQ) 1 H- 13 C methyl-CPMG (Carr-Purcell-Meiboom-Gill) experiments produce relaxation dispersion (RD) curves in which the effective transverse relaxation rate R_2^{eff} is measured as a function of the frequency at which refocusing CPMG pulses are applied, ν_{CPMG} . The resulting values are determined by the intrinsic relaxation rate R_2^{0} and a term R_{ex} that quantifies additional relaxation arising from dynamic exchange

between states with different chemical shifts that occurs on the time scale of the refocusing CPMG pulse train (μ s-ms), $R_2^{\text{eff}}(\nu_{\text{CPMG}}) = R_2^0 + R_{\text{ex}}(\nu_{\text{CPMG}})$. Fitting the resulting RD curves to a k_A

two-state exchange model, $A \stackrel{\rightarrow}{\leftarrow} B$, produces values for the rate of exchange between the two k_B

states $k_{ex} = k_A + k_B$, their relative populations, $p_A = \frac{[A]}{[A] + [B]} = \frac{k_B}{k_A + k_B}$, and the chemical shift differences between the exchanging states $|\Delta \omega_C|, |\Delta \omega_H|$. In the fast exchange limit, where $k_{ex} \gg \Delta \omega$, the best-fit $|\omega_C|, |\omega_H|$, and p_A values becomes unreliable as many combinations of these parameters can yield equally good fits, and only the k_{ex} values can be interpreted [36]. In the case of a global two-site exchange, wherein all signals are experiencing the same exchange process, the RD curves may be "globally fit", with shared parameters p_A and k_{ex} [37].

Measurable relaxation dispersion was observed for all of the Thr and Ile methyl probes in apo

TRAP (Figure 3, Figure 4, Figure S 2, Figure S 3). Fitting the RD curves showed all methyl probes to be in the fast exchange regime $(k_{\rm ex} >> \Delta \omega)$ and therefore preclude separate quantification of the p_A and $\Delta\omega$ [38,39]. The RD curves for all six threonine and three of the Ile δ_1 methyl groups (Ile26, Ile53, Ile61) could be globally fit to a single two-state exchange process with $k_{\rm ex} = 1700 \pm 300 \, {\rm s}^{-1}$ These residues map to the Trp binding loops and the core of the TRAP protomer (Figure 4B). Three of the four remaining Ile residues (20, 43, 68), which map to the inter-protomer interfaces, could be globally fit to a separate two-state exchange process with $k_{\rm ex} = 2100 \pm 300 \, {\rm s}^{-1}$. Including Ile10 in this global fitting resulted in large residuals so it was fit individually with a unique $k_{\rm ex}$ =

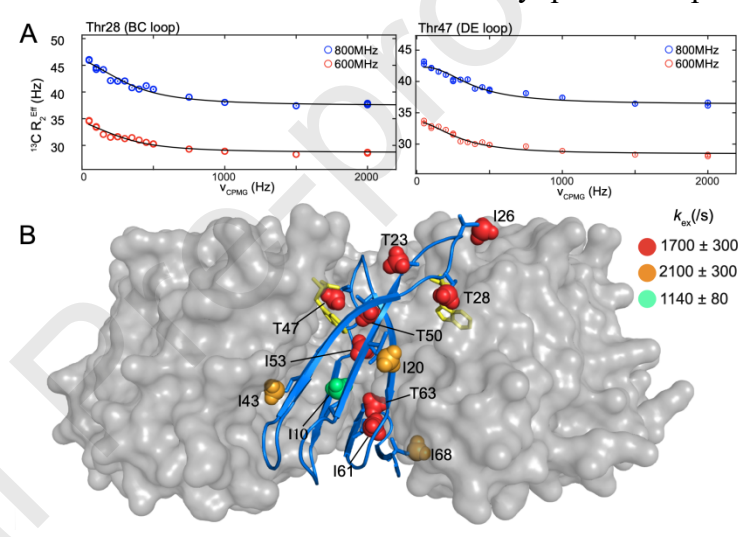


Figure 4: Methyl 13 C relaxation dispersion profiles of apo-A261-TRAP reveal both concerted and distinct motional modes. (A) MQ RD curves for methyl groups on the BC loop (Thr28, left) and DE loop (Thr47, right) can by fit with the same two-state exchange rate $k_{\rm ex}$ of $1700 \pm 300~{\rm s}^{-1}$. (B) Three distinct motional modes could be inferred from fitting of the RD curves. The Thr and Ile 26, 53 and 61 methyls form one group (red), Ile 20, 43 and 68 (orange, 2100 \pm 300 ${\rm s}^{-1}$) form a second group, leaving one Ile110 (green, $1140 \pm 80~{\rm s}^{-1}$) with unique exchange properties.

 1140 ± 80 s⁻¹. Upon binding Trp, the RD profiles are flattened for all except the methyl groups in the interprotomer interface (Figure S 4).

Methyl Order Parameters

To complement the measurement of μ s-ms dynamics in apo-TRAP, we performed methyl dipole-dipole cross-correlated relaxation measurements to quantify the amplitude of fast motion experienced by the methyl bond axis [40,41]. These experiments quantify motion via the generalized order parameter S^2 , where a high value ($S^2 = 1.0$) corresponds to a rigid bond vector

on time scales faster than overall tumbling (for TRAP, τ_c = 32 ns) and a low value (S^2 = 0.0) corresponds to unconstrained motion about the bond vector [42,43]. Intensity ratios for double-quantum and single-quantum coherences were generated from the ^1H - ^1H dipolar cross-correlated

relaxation experiments [42] at 55 °C for all Thr and Ile methyl groups in apo A26I-TRAP and fit with a relaxation rate (η) from which we extracted the generalized order parameter (S^2 ; see Methods) (Figure S 6, Figure S 7). We found that apo-TRAP exhibits large amplitude of motions on the ps-ns timescale as indicated by an average order parameter of ~0.5 (Figure 5; Table 1). Methyl groups from Thr28, Thr47 and Thr50 in the BC and DE loops have low order parameters with S^2 of 0.33, 0.27, and 0.53, compared to an S^2 of 0.99 for Thr63 which is located on β strand F

Resi	Residue	S^2	
3	Thr	0.36 ± 0.06	
10	Ile	0.56 ± 0.05	
20	Ile	0.43 ± 0.02	
23	Thr	0.83 ± 0.03	
26	Ile	0.24 ± 0.01	
28	Thr	0.33 ± 0.01	
43	Ile	0.49 ± 0.07	
47	Thr	0.27 ± 0.01	
50	Thr	0.53 ± 0.07	
53	Ile	0.52 ± 0.06	
61	Ile	0.68 ± 0.04	
63	Thr	0.99 ± 0.12	
68	Ile	0.26 ± 0.01	

Table 1: Methyl Order Parameters for A26I-apo-TRAP, obtained from fitting intensity ratios of peak intensities in single- and double-quantum cross-correlated relaxation experiments [42].

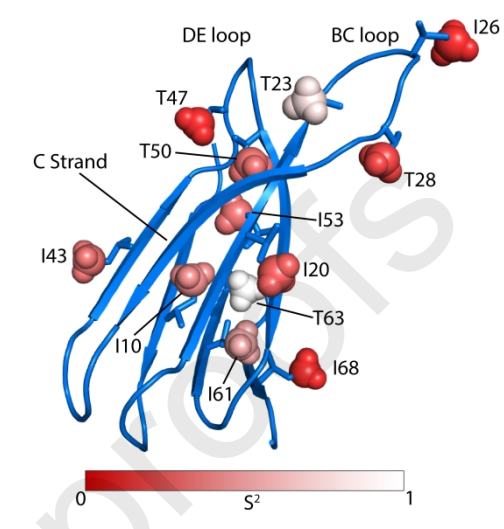


Figure 5: Methyl axis order parameters S² reveal a high degree of conformational flexibility in both the solvent exposed loops and hydrophobic core of A26I-TRAP. Fitted Thr/Ile methyl S² order parameters (Table 1) for mapped to a single protomer of the crystal structure of Trp-bound TRAP. Thr residues in the binding loops exhibit very low S² < 0.4. Thr63 exhibits a particularly high order parameter as is anticipated since this residue is in the rigid core of the protein. (Thr3 was not resolved in the crystal structure and is not shown.)

at the core of the protein. This indicates that the Thr

residues in the loops are overall more flexible on the ps-ns time scale than those in the rigid core. Unexpectedly, Thr23 in the BC loop exhibits a relatively high order parameter of 0.83 despite in a loop predicted to be flexible based the absence of backbone resonances for that region [24]. Thr3, at the unstructured amino terminus also exhibits a low S^2 (Table 1).

Solid-State NMR Backbone and Side-Chain Resonance Assignments

To extend the backbone and side-chain resonance assignments for apo TRAP we conducted solid-state NMR experiments on uniformly ¹³C, ¹⁵N-labeled wild-type TRAP. Prior solution NMR studies of apo-TRAP, at 55 °C and 800 MHz, yielded resonance assignments for only ~49% of the protein backbone due to absence of many signals in correlation spectra stemming from conformational exchange. While solution NMR experiments were conducted at elevated temperatures to increase the overall molecular tumbling rate and obtain narrower resonance widths [24,25], because linewidths in solid-state NMR experiments are independent of the rotational correlation time [28] we reasoned that by recording NMR spectra in the solid-state at lower temperatures we may be able to freeze out motions that lead to broadening and

Journal Pre-proofs

disappearance of NMR signals [37]. Specifically, we recorded a set of cross-polarization (CP) based triple-resonance experiments on apo TRAP at 4 °C and 800 MHz, including 3D NCACX, NCOCX, and CANCO[44], to establish sequential resonance assignments. Comparison of the $^{15}\text{N-}^{13}\text{C}$ projections from solution-state TROSY-HNCA recorded at 55 °C and solid-state NCACX spectra show good agreement (Figure 6) with average $\Delta\delta$ for ^{15}N amide and $^{13}\text{C}\alpha$ shifts of 0.16 and 0.07 ppm, respectively. In addition, DARR spectra recorded at 45 °C show minimal chemical shift perturbations compared to 4 °C, indicating that the structure of the rigid core remains unperturbed, consistent with the above noted comparisons of solid-state and solution state NMR spectra recorded at 4 °C and 55 °C (Figure S 8).

Backbone ¹³C and ¹⁵N resonance assignments could be unambiguously established from the

NCACX, NCOCX, and CANCO spectra for 40 out of 74 residues (Figure 6). Additionally, these spectra enabled assignment of several side chain ¹³C resonances that were not accessible from solution NMR data. Chemical shift-based secondary structure prediction with TALOS-N[45] shows that the residues observed in CP-based experiments adopt the same secondary structure that is seen in crystals of holo-TRAP. Signals for residues 9-20, 36-44, and 53-70 all were assigned in solid-state spectra of apo TRAP and are predicted from their shifts to adopt either a β-strand or loop conformations.

The CP-based solid-state experiments recorded at 4 °C reveal that dynamic disorder persists at the reduced temperature. Notably, several signals expected for the 74-residue protein are absent in the C^{α}/C^{β} region of a 2D ¹³C-¹³C DARR spectrum (Figure 7B). For example, only one threonine (Thr63) out of the six exhibits detectable C^{α} - C^{β} and C^{β} - C^{γ} correlations, and in the alanine region only three of the five correlations are observed, the other correlation in that region arises from a leucine side chain. Aromatic sidechain correlations are observed only for His65 and Tyr60 in the rigid core on β -strand F (Figure 7B).

Given that DARR, NCACX, NCOCX, and CANCO experiments rely on dipolar coupling-based magnetization transfers, the assigned regions correspond to the

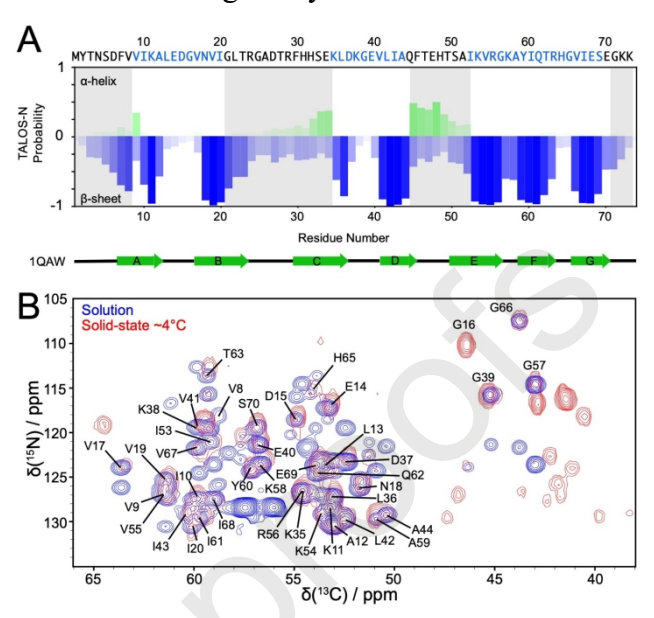


Figure 6: Solid state NMR data of apo TRAP are consistent with solution measurements. (A) TALOS-N secondary structure prediction from chemical shifts assigned in solid-state at 4°C. Primary sequence above with annotation of secondary structure observed in holo TRAP crystal structure. (B) Solution- and solid-state NMR spectra are consistent with local dynamic disorder. Overlay of solution 800 MHz TROSY-HNCA spectrum (blue) with 2D projection from the 3D solid-state MAS NCACX spectrum (red) recorded at the indicated temperatures. Backbone resonance assignments as indicated, unlabeled blue signals correspond to i-1 correlations and unlabeled red signals correspond to sidechain chemical shifts. Close agreement between solution and solid-state spectra indicates similar structures under both conditions. Additional signals in the solid-state spectrum are from aliased Lys/Arg sidechain resonances or C^{β}/C^{γ} correlations from sidechain amides of Asn and Gln. Line widths for 13 C in the NCACX are ~ 1 ppm, indicative of a well folded protein. Approximately 50% of possible N- C^{α} correlations are visible in the solid-state experiment.

rigid core of apo TRAP. In addition, several other residues in the structured regions of holo TRAP did not have observable resonances in the CP-based solid-state NMR spectra of apo TRAP. Residues 30-34 in the C-strand, 23-28 in the BC loop, and 46-49 in the DE loop, were "invisible" in conventional CP-based experiments; their absence likely arises from the motional averaging of the dipole-dipole couplings that are required for magnetization transfer[46]. To complement the CP-based solid-state NMR experiments described above and extend our NMR analysis to the flexible regions of apo TRAP we used INEPT-based NMR experiments recorded under MAS which are mediated by scalar (*J*) coupling interactions not averaged by isotropic or

near-isotropic local motions[47]. This permits observation of signals arising from the most dynamic regions of the protein while 'filtering out' signals arising from the rigid core residues. ¹³C-detected refocused INEPT[48] experiments show an increase in signal from 4°C to 45°C, consistent with an increase in local protein dynamics (Figure S 9).

The INEPT-based ¹H-¹³C correlation spectrum recorded at 45 °C contains a number of intense

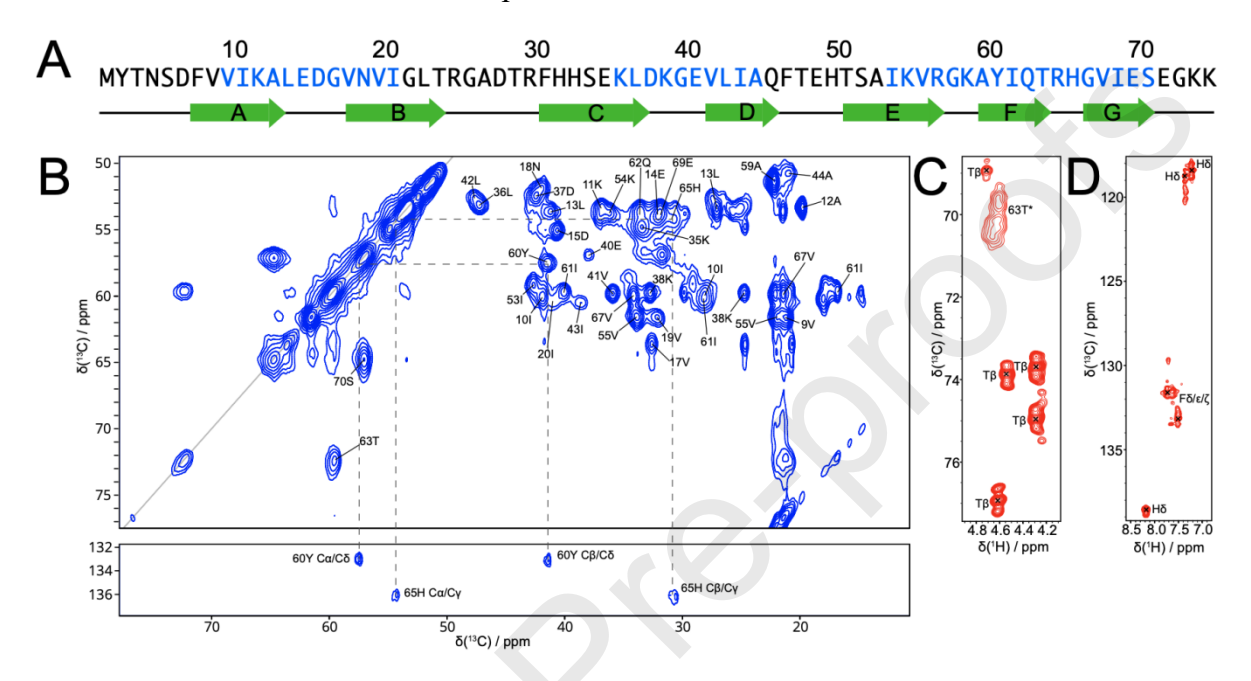


Figure 7: CP- and INEPT-based spectra distinguish structured and flexible regions of apo TRAP. (A) Primary sequence of TRAP. Residues in blue produced signals in solids CP-based experiments. (B) 13 C- 13 C DARR spectrum with 50 ms mixing time at 11 kHz MAS, 800 MHz field [U- 13 C, 15 N]-apo-TRAP. The alanine C^{α} - C^{β} region only shows three of the five alanine resonances (12, 44, 59). Correlations are observed for only one of the six Thr, Thr63. (C) 13 C-detected 2D INEPT spectrum shows five distinct sets of Thr C β -H β correlations, with typical one bond C^{α} - C^{β} J-coupling values of \sim 34 Hz. The broad peak 63T* corresponds a minor state of the C β -H β correlation of Thr63 seen in panel B. (D) Aromatic region of the 2D INEPT showing histidine and phenylalanine sidechain correlations.

correlations from the aromatic and aliphatic regions of residues such as Thr, His, and Phe located outside of the rigid core (Figure 7 C,D). Specifically, this spectrum shows five signals with H^{β} and C^{β} chemical shifts that can only be attributed to Thr residues, with ~35 Hz 13 C J-couplings[49]. There is an additional signal at ~70 ppm that is broadened compared to the other Thr resonances which we assign to Thr63, consistent with broadening that is also seen in the DARR spectrum (Figure 7B). The aromatic region of the spectrum reveals $^{1}H^{-13}$ C correlations representative of His and Phe sidechain carbons (120 ppm and 130 ppm, respectively). These aromatic signals can only come from residues 30-32 in the C-strand or 46 and 49 in the DE loop, supporting the conclusion that the C-strand undergoes significant motions in apo TRAP.

Apo TRAP Sidechain Rotamers

The chemical shifts of C^{α} , C^{β} , $C^{\gamma 1}$, $C^{\gamma 2}$, and C^{δ} nuclei from all IIe residues (10, 20, 43, 53, 61, and 68) in both apo and holo TRAP were assigned from 2D and 3D solid-state NMR spectra [50] (Figure S 10). Spectra for holo TRAP, recorded at 1.2 GHz, were sufficiently resolved to enable

assignment from 2D spectra alone, while 3D spectra were required for assignment of apo TRAP, recorded at 800 MHz. Notably, MAS NMR spectra of Trp-bound TRAP featured narrower lines and a more complete set of resonances than the same spectra of apo-TRAP (Figure S 11). Ile resonance assignments were used to predict the populations of the $\{\chi_1, \chi_2\}$ rotameric states by reference to chemical shifts predicted for discrete rotameric states [51] in the fast-exchange regime [52]. Based on these data, Ile residues 10, 20, 43, 53, and 61 in apo TRAP are predicted to sample at least two rotameric states (Figure 8) with the major state (having a probability >0.5) being $\{g/t\}$ (gauche-/trans). Ile 20, 43, and 53 exchange between three separate states ($\{g/t\}$, $\{g_+/t\}$, and $\{g_-/g_-\}$), whereas Ile 10 and 61 only exchange between two states. Comparing the rotamer distributions predicted for apo TRAP with those predicted for holo TRAP reveals mostly modest changes in the rotamer distributions. For Ile43, the most dominant rotameric state shifts from $\{g_{-},t\}$ to $\{g_{+},t\}$, more closely resembling a random coil distribution as noted by the large $\{g_+,t\}$ and low $\{g_-,t\}$ populations [53]. Ile53, which forms a complementary hydrogen bonding interaction with Ile43 in the βE-βD inter-protomer interface, sees a small increase in its favored $\{g_{\cdot,t}\}$ state and resembles a β -strand distribution. By comparison, in holo TRAP crystals (1QAW, 1C9S, 1GTF, with resolutions down to 1.75 Å), all Ile residues are modeled as adopting the $\{g_{-},t\}$, except Ile68 which was modeled in the $\{t,t\}$ conformation [19]. The ligand-induced chemical shift changes are thus suggestive of population shifts that from binding-coupled changes in the free energy landscape of the protein.

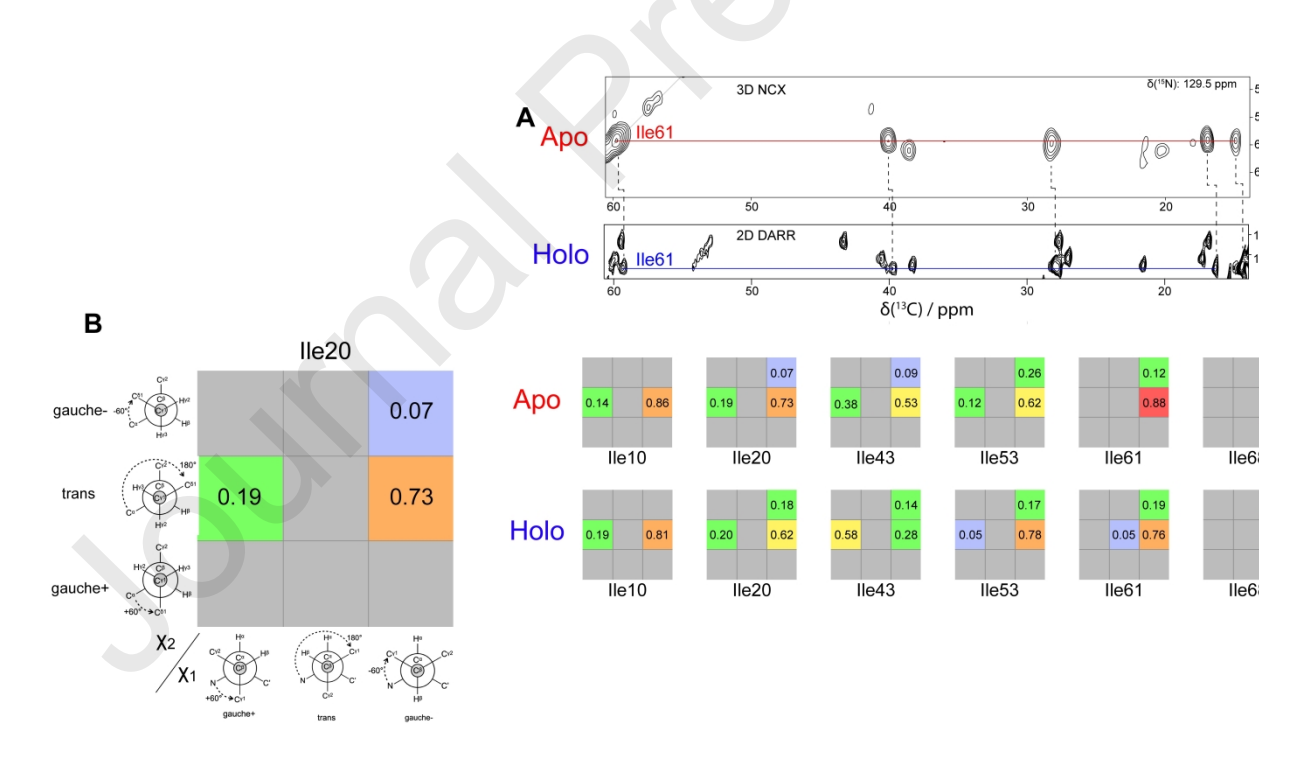


Figure 8: Trp binding results in altered rotamer distributions for Ile side chains. (A) Top, 2D slice from NCACX spectrum collected at 800 MHz of apo TRAP. Red-line passes through cross-peaks that arise from C^{α} correlations to the side chain carbons. Bottom, strip from DARR spectrum collected at 1.2 GHz of holo TRAP. Blue-line passes through cross-peaks that arise from C^{δ} correlations to the rest of the side chain. (B) Left, schematic of rotamer distribution graph. Right, rotamer distributions for Ile residues were calculated from the sidechain 13 C chemical shifts.

Discussion

This study builds upon prior solution NMR studies of TRAP [24,25], a 91 kDa homo-oligomeric ligand-activated gene-regulatory protein, with the goal of advancing a mechanistic understanding of its activation by Trp. Introduction of Thr methyl labeling allowed us to probe the dynamics of residues in the BC and DE loops that are directly responsible for chelating the Trp ligand and not just distal sites in the hydrophobic core. Application of solid-state NMR methods allowed us to extend resonance assignments of apo TRAP thereby illuminating how ligand-coupled conformational changes influence subsequent binding events, giving rise to its positive homotropic cooperativity [21,22]. These findings build upon and extend previous understanding of the mechanism of Trp binding, cooperativity and activation of TRAP.

Concerted motions gate Trp binding

Our methyl ¹³C CPMG relaxation dispersion data support a model in which internal motions in apo TRAP allow it to transiently sample conformations that facilitate Trp binding (Figure 9). All of the Thr and Ile methyl groups in apo TRAP exhibit relaxation dispersion in ¹³C CPMG experiments (Figure 4, Figure S 2, Figure S 3) [25], indicating dynamics on the μs-ms time scale. In prior NMR relaxation experiments conducted with ILV-methyl labeled A26I-TRAP [25], the single probe on the BC loop, Ile26, exhibited fast exchange dynamics, but the remaining methyl RD curves from Ile, Leu and Val residues in the core of the protein could not be reasonably fit with a global two-state exchange process. This finding was interpreted to indicate that apo TRAP experiences *asynchronous* conformational sampling at the protomer level, reducing the likelihood of multiple adjacent protomers adopting a binding-competent conformation.

The present data, recorded on instruments capable of higher frequency refocusing pulses, with methyl probes that directly report on the dynamics of the Trp binding loops, paint a more precise picture of loop dynamics in TRAP. We found that 13 C RD curves for the six Thr γ_2 methyls and

seven Ile δ_1 methyls could be fit with three separate two-state exchange models. Methyl ¹³C RD Curves for the six Thr and three of the Ile methyls were globally fit with a $k_{\rm ex}$ of 1700 s⁻¹. Exchange dynamics are almost entirely quenched for these residues in the presence of Trp (Figure S 4). This set of methyl groups is concentrated in the BC and DE loops, and in the core of the protein (Figure 4). With $\Delta\omega$ for ¹³C methyl groups not exceeding \sim 200 Hz (\sim 1 ppm at 800 MHz), the fitted exchange rate is in the fast limit, convoluting the minor state populations and their chemical shifts. Nevertheless, since the Trp binding sites are occluded in the Trp-bound crystal structures and the rate of Trp binding to TRAP is vastly

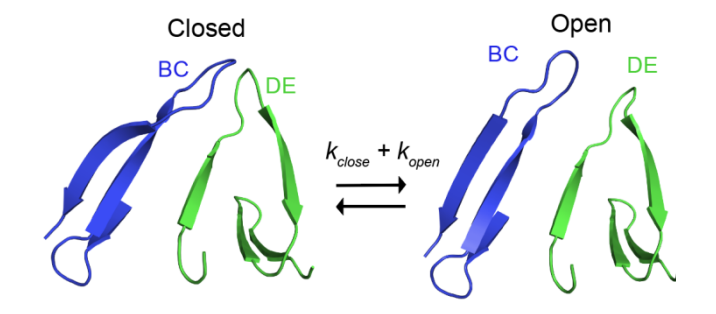


Figure 9: Model for concerted conformational exchange mechanism for gating access to Trp binding sites. Exchange between open and closed conformations on a rate $k_{\rm ex} = k_{\rm open} + k_{\rm close}$ on the sub-millisecond timescale leads to the observed methyl relaxation dispersion in ¹³C CPMG experiments. Because Trp binding is much slower than diffusion, the open state is thought to be short-lived and lowly populated.

slower than the diffusion limit [19,54], we interpret exchange process to reflect concerted

sampling of a transiently populated "open" conformation of the binding loops, which could permit entry of Trp (Figure 9).

A second set of methyl groups ms timescale exchange that is similar in both apo and Trp-bound TRAP. RD curves corresponding to Ile 20, 43, and 68, located at each inter-protomer interface, were globally fit with $k_{\rm ex}$ of 2131 s⁻¹. Finally, Ile10 in the hydrophobic core was fit individually with a $k_{\rm ex}$ of 1138 s⁻¹. These findings show that exchange on the μ s-ms time scales is prevalent in TRAP and could be a consequence of its oligomeric ring-shaped structure, and could possibly play a role in stability and/or RNA binding.

The Free Energy Landscape of Apo TRAP is Rough and Broad

These solid-state and solution-state NMR spectra expand our understanding of dynamics in apo TRAP. As noted above, methyl relaxation dispersion data for the Trp binding loops provided evidence for concerted μ s-ms timescale fluctuations that are quenched upon ligand binding, and a separate set of conformational μ s-ms exchange processes that persist in the presence of ligand. We extend those insights by quantifying methyl dynamics on faster time scales via the generalized order parameter S^2 , which reports on the amplitude of methyl-axis reorientation motions on the ps-ns timescale. Finally, ¹³C chemical shift data for Ile residues, obtained from solid-state measurements provided insights into conformational sampling of rotameric states on time scales faster than those measured by CPMG methods.

Cross-correlated methyl relaxation NMR experiments (Figure 5, Table 1) show that apo TRAP is dynamic on the ps-ns timescale. Apo A26I-TRAP has many methyl groups with low S^2 order parameters indicative of large amplitude methyl axis reorientation. Moreover, Ile and Thr methyl groups exhibit dramatically different S^2 values, despite exhibiting similar μ s-ms motions (Figure S 2). Thr63 is interesting as it could be globally fit to the same two-state exchange process as the other Thr residues but exhibits a high order parameter in ($S^2 = 0.99$) indicative of rigidity on the timescale of molecular tumbling. This is consistent with the unique appearance of the Thr63 methyl signal in both the CP-based and INEPT-based solid state NMR spectra (Figure 7). Interestingly, this residue is highly conserved across bacterial species [55], and in crystal structures the sidechain $O\gamma_2$ is observed to hydrogen bond to the amide of His65 in the tight β FG turn [19,56], so its rigidity on the fast timescales may reflect a role in stabilizing local fold of the protein.

The solid-state NMR spectra provide further support for a conformationally variant apo TRAP protein. Cross-polarization NMR methods make use of strong dipolar couplings to transfer magnetization between spins and generate correlations in multidimensional spectra [57,58]. Internal motions result in reorientation of dipoles relative to the static magnetic field, which in turn leads to averaging of the dipolar couplings and loss of signal in CP-based spectra. Conversely, the same rapid dynamics enables preservation of transverse magnetization and observation of signals in INEPT-based spectra of solids [47]. As such, the observation of intense signals in MAS INEPT-based spectra corresponding to the Thr residues in the BC and DE loops, as well as for the His and Phe residues in the DE loop (Figure 7), is strongly suggestive of those regions of the protein being highly flexible, even at 4 °C in the solid state. In total, backbone resonance assignments could be obtained by solid-state NMR for 40 out of the total 74 residues of apo TRAP; these are consistent with those obtained previously from solution experiments at

55 °C and correspond to the well-structured rigid core of the protein rings. Absence from the CP-based spectra of signals from the amino terminus, BC and DE loops, and C-terminal residues (Figure 6), is indicative of their disorder and flexibility in the solid state.

Trp Binding Results in a Shift in the Free Energy Landscape

Chemical shift data provide rich structural information about differences between apo and holo TRAP. Comparison of methyl spectra of A26I-TRAP in the absence and presence of Trp (Figure 3) reveal perturbations in both the ¹H and ¹³C shifts, indicative of changes in the local environment experienced by these methyl probes. In the absence of Trp four of the six Thr methyl resonances have nearly degenerate ¹³C chemical shifts (~21.5 ppm), while Trp binding disperses these resonances ~1 ppm (Figure 3).

The solid-state NMR experiments allowed us to extend these analyses beyond the Thr and Ile methyl groups. Two-dimensional $^{13}\text{C-}^{13}\text{C}$ DARR spectra of apo TRAP contain fewer and broader signals in the aliphatic region (50-60 ppm) and side-chain methyl region (10-20 ppm) in comparison to holo TRAP (Figure S 11). These narrower signals and additional signals may result from increased static order and decreased motional averaging of the $^{13}\text{C-}^{1}\text{H}$ and $^{1}\text{H-}^{1}\text{H}$ dipolar couplings accompanying Trp binding. Additionally, the Thr $\text{C}\alpha/\text{C}\beta$ and $\text{C}\beta/\text{C}\gamma$ region in holo TRAP spectrum (Figure S 11) contains four additional signals that were not observed in the CP-based spectrum of apo TRAP. These additional signals result from rigidification of the BC and DE loops upon Trp binding.

NMR resonance assignments of Ile sidechains from solid-state spectra allowed interrogation of rotamer populations in apo and holo TRAP (Figure 8). Population distributions predicted from chemical shifts generally agree with those modeled in the holo TRAP crystal structures. In those structures, from crystals that diffracted to a resolution of 1.75 Å, all Ile sidechain χ_1 and χ_2 torsion angles were observed to adopt $\{g_{..}t\}$ configurations, except for Ile68 which is present as the $\{t,t\}$ rotamer [19,56]. Comparing the ¹³C chemical shifts of the Ile sidechains from solid-state NMR spectra of apo and holo TRAP (Figure 8) suggests that Trp binding only modestly alters the rotamer distributions. This result contrasts with the large differences in methyl CPMG relaxation dispersion profiles that reveal large effects on conformational sampling on the ms timescale. Because the chemical shifts arise from rotameric interconversion that can be much faster than the ms exchange detectable by CPMG experiments [59–61], these results indicate that in the slowly exchanging states the sidechains of these residues rapidly sample the available rotameric states with a similar distribution. Nevertheless, even modest shifts in the free energy landscape can contribute significantly to the thermodynamics of ligand response [62].

Cooperativity from Population Shifts Upon Initial Trp Binding

Positive thermodynamic cooperativity dictates that after one ligand binds, subsequent binding events may occur with higher affinity, as measured by the equilibrium constant K between the free and ligand-bound states. This cooperativity can be quantified from the free energy difference between binding events $\Delta\Delta G = -RT \ln \alpha$, where $\alpha = K'/K$ is the observed fold change in affinity for subsequent compared to initial binding. Ligand titrations monitored by calorimetry and native mass spectrometry, and analyzed with a nearest-neighbor Ising model [21,22], reveal that Trp binding to TRAP is modestly cooperative with $\Delta\Delta G$ coupling energies between adjacent sites of

about -1 kcal mol⁻¹, or ca. -1.7 RT. Understanding the basis for Trp-Trp cooperativity in TRAP requires identifying the origins of this thermodynamic difference between initial and subsequent binding events.

The NMR data presented and analyzed here do not allow us to directly observe Trp-Trp cooperativity, as they only allow us to determine and compare properties of the two extremes, the empty apo- and fully bound holo-states of the protein. Under suitable conditions, such insights into cooperativity can be inferred from NMR titrations, even for rather complex systems [63]. However, we note that an underlying complexity for these studies is that with 11 binding sites for Trp, there exist $2^{11} = 2048$ possible configurations of TRAP with 0-11 bound Trp; after accounting for symmetry there are still 32 energetically distinct configurations [22]. For instance, addition of just one equivalent of Trp would result in statistical mixtures of rings 0-11 bound, with the populations of states strongly dependent on the extent of cooperativity [21,64]. Consequently, except in the case of extreme cooperativity, the observed NMR signals would arise from averaging of many possible configurations. Absent detailed measurement of intermediate states, we considered what might be learned about the basis of cooperativity from comparison of apo and holo states of the protein.

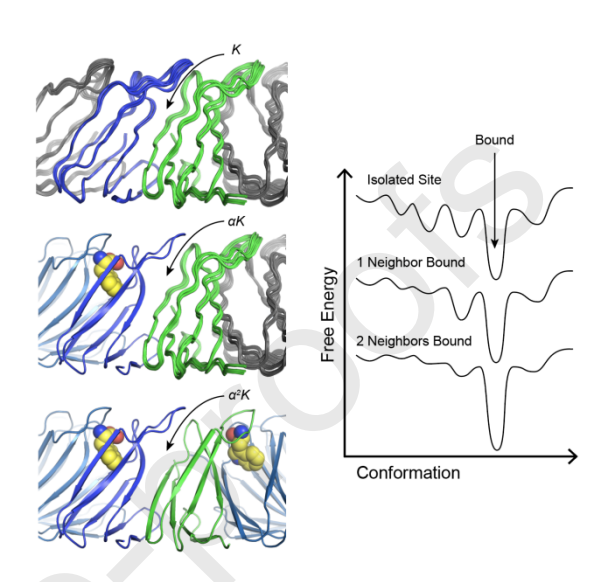


Figure 10. Model for conformational shift in Trp-Trp cooperativity in TRAP. For an isolated Trp binding site i with no bound neighbors, the free energy landscape is shallow and rough, with many conformational states being populated. The binding equilibrium constant K reflects the free energy penalty of generating order in the site. Binding of Trp to an adjacent site i-1 reduces conformational sampling a site i, resulting in a more favorable affinity αK . Trp binding at both adjacent sites further narrows the free energy landscape, resulting in more favorable Trp binding.

We favor a model in which Trp-Trp cooperativity in TRAP results from reduced conformational sampling (dynamics) at adjacent sites upon initial binding, driving a population shift that favors subsequent ligand binding events (Figure 10). We may consider that the free energy landscape of an individual ligand-free site *i* can be described as rough and shallow, with many conformations being similarly populated, including one that resembles the bound state. If binding of a ligand to a neighboring site *i*-1 results in narrowing of the free energy landscape at site *i*, this can favor binding at site *i* by both enthalpic and entropic means. First, reducing the population of binding-incompetent states for site *i* results in a lower enthalpic penalty for ordering the site [65,66]. Second, if binding at site *i*-1 induces in site *i* a lower population of states, a smaller entropic penalty must be paid upon binding to adopt a bound configuration.

This model is supported by several observations from the current study. First, as measured by ¹³C RD, ¹H-¹H cross-correlated relaxation experiments, and solid-state CP and INEPT-based NMR experiments, the Trp binding sites in apo TRAP feature a high degree of temporal disorder (dynamics). RD profiles from Ile and Thr methyl groups exhibit exchange on ms time scales, and much of these dynamics are quenched upon Trp binding. Order parameters for the Ile and Thr

residues for apo TRAP are low compared to other characterized globular proteins, whereas reduction in those degrees of freedom upon ligand binding would necessarily incur an entropic penalty that would have to be balanced by other favorable interactions [8,67–70]. Residues Thr 23, 28, and 47 have particularly low S² values (<0.4) in apo TRAP, which is indicative of a high degree of conformational entropy [69,71]. Thus, activation of TRAP by Trp could involve extensive conformational restriction; this is supported by a large experimentally measured negative heat capacity change ΔC_p upon Trp binding [22].

Although binding entropy is often dominated by changes in solvent accessible surface area [66,72], the contribution of conformational entropy changes to total binding entropy change can in principle be estimated from changes in NMR order parameters [15,70]. Because we were not able to experimentally measure methyl axis order parameters for Thr and Ile residues in holo TRAP we instead used parameters predicted by a contact model from the 1.9 Å crystal structure of Trp-bound TRAP (1C9S) [19]. By approximating methyl axis motion by diffusion in a cone, changes in the S^2 values were used to estimate the change in protein conformational entropy (ΔS_{conf}) associated with Trp binding [73]. These calculations yield an entropic cost for ordering a site of ca. RT (~3 kcal mol⁻¹ at 40 °C) that would have to be compensated for by favorable changes in enthalpy and/or solvent entropy. This value is on the same scale, though opposite sign, as the calorimetrically-measured $\Delta S_{\text{coupling}}$ of +8 RT (+5 kcal/mol), which represents the change in entropy associated with occupying a neighboring site [22]. Additional entropic costs from conformational changes would be expected from redistribution of the Ile rotamer populations, although most populations changed by less than 0.2 (Figure 8). While this analysis fails to elucidate a unique set of contributions to Trp-Trp cooperativity, the findings of reduced dynamics, and shifts in population of sidechain conformations, are consistent with the population shift model of allostery (Figure 10).

Conclusion

Overall, these findings significantly advance our understanding of the functional implications of ligand-altered dynamics in TRAP. TRAP functions as sensor of Trp in cells, and the ligand should modulate the RNA binding activity of TRAP over a physiologically useful concentration of its ligand. The methyl RD data of apo TRAP are consistent with a model in which concerted gating motions in the Trp binding loops enable TRAP rings to sample conformations that enable binding. Insights into Trp binding cooperativity can also be inferred from comparison of the structural and dynamic data between apo- and holo-TRAP. Given that ligand binding is accompanied by local protein restriction, this implies an unfavorable conformational entropy change. If initial binding results in reduction in conformational sampling of neighboring sites, favoring a bound-like conformation subsequent binding events will be accompanied by a more favorable ΔH and a smaller ΔS penalty. Thus, the observed conformational narrowing could provide a mechanistic explanation for the observed NN cooperativity in Trp binding in TRAP.

Methods

Sample Preparation

NMR experiments were performed with either wild-type (WT) Gst TRAP, and a point mutant in which Ala26 was replaced with Ile (A26I-TRAP) to provide an additional methyl probe on the BC loop. For each sample, data were recorded in the absence and presence of Trp. NMR samples were recombinantly expressed from Escherichia coli grown in defined minimal media. Trp-free apo TRAP was purified under denaturing conditions to ensure complete removal of Trp, as described previously. Solid-state NMR spectra were recorded with U-[1H, 13C, 15N]-TRAP (WT), while the Thr and Ile [13CH₃], U-[2H,15N]-A26I-TRAP was used for solution-state spin relaxation measurements and HCH/CCH methyl-methyl NOESY for assignments. Isotopic labeling of the sample used for solid-state NMR studies was accomplished by protein expression in E. coli BL21(DE3) cells grown on M9 minimal media containing ¹⁵NH₄Cl and ¹³C-glucose as the sole nitrogen and carbon sources, respectively. Ile and Thr methyl-labeling was accomplished using perdeuterated metabolic precursors of Thr and Ile. A26I-TRAP was used for solution NMR experiments for consistency with prior spin relaxation experiments; samples were 1 mM A26I-TRAP (monomer) in NMR buffer (100 mM NaCl, 50mM NaPO₄, pH 8.0, 10% D₂O). WT TRAP was used for solid-state experiments in NMR buffer without D₂O. For visualization, PyMOL (http://pymol.org) was used to introduce the Ile26 to Ala mutation using either the 1QAW or 1C9S holo structures as templates.

Solution NMR Spectroscopy

Spectra were recorded on Bruker Avance III HD 600 and 800 MHz spectrometers equipped with HCN z-axis gradient cryo-probes. Sample temperatures were calibrated using a methanol standard and chemical shifts were referenced externally to DSS.

Thr methyl signals of apo A26I TRAP were assigned using two spectra of A26I-TRAP recorded at 55 °C: HCH Methyl-Methyl NOESY to correlate a ¹H-¹³C pair to a neighboring methyl ¹H, and CCH Methyl-Methyl NOESY to correlate another ¹H-¹³C pair to neighboring ¹³C spins [34].

For both apo and holo A26I-TRAP ¹³C multiple-quantum methyl CPMG experiments were carried out at 20 °C. Dispersion curves for apo TRAP were obtained using interleaved CPMG field strengths of 50, 100, 150, 200, 250, 300, 350, 400, 450, 500, 750, 1000, 1500, and 2000 Hz and 50-4000 Hz for holo TRAP.

Dispersions were calculated using $R_2^{\rm Eff}$ = -ln($I(v_{CPMG})/I_0$)/ I_{CPMG} , where $I(v_{CPMG})$ is the signal intensity from a spectrum with a refocusing duration of I_{CPMG} at a given frequency and I_0 is the intensity from the spectrum without refocusing pulses. Peak intensities were measured and converted to transverse relaxation rates ($I_0^{\rm Eff}$) using NMRPipe [74]. The GUARDD software package was used to fit the relaxation dispersions to the Carver-Richards equation that describes the relaxation contribution from chemical exchange ($I_0^{\rm Eff}$) to transverse relaxation ($I_0^{\rm Eff}$) by fitting an exchange rate ($I_0^{\rm Eff}$) and population ($I_0^{\rm Eff}$) for two-state exchange [75]. Errors for fitted parameters were determined by grid searching a five-dimensional parameter space to minimize $I_0^{\rm Eff}$ 0. Dynamics in the fast exchange regime limited the determination of $I_0^{\rm Eff}$ 1 and $I_0^{\rm Eff}$ 2 and $I_0^{\rm Eff}$ 3 are regime limited the determination of $I_0^{\rm Eff}$ 3.

any combination of the three can provide equally good fit to $k_{\rm ex}$ when assessed by χ^2 analysis. Methyl probes that fit for similar parameters were fit to a global model.

Methyl order parameters (S^2) for Ile and Thr residues in A26I-TRAP were obtained from measurement of the intensity ratios of double-quantum and single-quantum coherences generated from $^1\text{H-}^1\text{H}$ dipolar cross-correlated relaxation experiments[42] using a pseudo-3D spectrum. Data were recorded at 55°C at which previous studies established a correlation time τ_c = 34.2 ns[76], using the following relaxation delays: 0.25, 0.5, 1, 2, 3, 4, 6, 8, 10, 12, 14, 16, 20, 30, 40, 50 ms. Peak intensities were extracted using NMRPipe and residue-specific S^2 values were obtained by fitting intensity ratios in Python using the lmfit library (https://lmfit.github.io/lmfit-py/). Uncertainties were obtained by from Mone-Carlo simulations using the spectral noise as the uncertainty in peak heights. S^2 parameters for Ile and Thr residues in holo-TRAP were computed for the 1.9 Å crystal structure 1C9S using a contact model [77,78]. S^2 parameters calculated from the holo TRAP structure and from $^1\text{H-}^1\text{H}$ dipolar cross-correlated relaxation experiments of apo TRAP were used to calculate the change in conformational entropy using a diffusion in a cone model [73].

Solid-State NMR Spectroscopy

MAS NMR spectra of U-[\(^{13}\text{C}\),\(^{15}\text{N}\)]-apo-TRAP were recorded on a Bruker Avance III HD 800 MHz spectrometer outfitted with an Efree HCN 3.2 mm MAS probe. Purified TRAP was sedimented in an ultracentrifuge at at 4°C and 100,000 rpm using a TLA 100.3 rotor. The protein precipitate was loaded into a 3.2 mm rotor using home-built tools in a tabletop centrifuge. The MAS frequencies were controlled within ±1 Hz by a Bruker MAS controller. The sample temperature was regulated by a Bruker VT controller and maintained at 4 °C throughout experiments as measured by a KBr external reference.

Typical ¹H, ¹³C, and ¹⁵N 90° pulse lengths were 2.5, 5.0, and 6.25 μs, respectively, and ~90kHz SPINAL-64 proton decoupling was applied during chemical shift evolution periods[79]. 2D ¹³C-¹³C DARR spectra were recorded at 11.111 kHz MAS rate and the following mixing times: 5, 15, 50, 100, and 500 ms, with a 11.111 kHz ¹H field applied during the mixing time[80]. 2D NCA, 2D NCO, 3D NCACX, 3D NCOCX, 3D CANCO· spectra were recorded at an MAS frequency of 11.111 kHz [80,81]. Band-selective CP (SPECIFIC-CP) [82] was used for magnetization transfer from ¹⁵N-¹³C in the NCACX and NCOCX, as well as for ¹³C-¹⁵N magnetization transfers in CANCO with 6ms and 6ms contact times respectively and 15 ms DARR was used for ¹³C-¹³C magnetization transfer in the NCACX and NCOCX experiments. A DARR spectrum of U-[¹³C,¹⁵N]-Holo-TRAP was recorded on a Bruker Ascend 1.2 GHz spectrometer outfitted with a 3.2 mm HX MAS probe, with sample temperature maintained at 4 °C.

A 2D ¹³C- refocused INEPT spectrum [48,83] was recorded with ¹H and ¹³C 90° pulse lengths of 2.5 μs and 5.0 μs, respectively. Spectra were recorded at 13 kHz MAS and sample temperature of 45 °C, determined from an inversion-recovery experiment on a KBr standard.

Resonance assignments for *Gst* TRAP have been deposited to the BMRB, accession XXXX.

Acknowledgments

The authors acknowledge the OSU CCIC NMR facility for access to instrumentation and expert support by Chunhua Yuan and Alex Hansen, and Vidhya Sridharan and Tanya Whitmer for advice in solid-state NMR data collection and processing. Paul Gollnick (University at Buffalo) provided reagents and indispensable advice. This work was supported by grants from the NIH (R01-GM120923 to MPF and PG) and from the National Science Foundation (MCB-2303862 to CPJ). Purchase of the 1.2 GHz NMR spectrometer used for some of the later solid-state NMR data collection was made possible from a Mid-scale RI-1 grant from the NSF (DBI-1935913). RM acknowledges support from NIH T32-GM086252. This study made use of NMRbox: National Center for Biomolecular NMR Data Processing and Analysis, a Biomedical Technology Research Resource (BTRR), which is supported by NIH grant P41GM111135 (NIGMS). Melody Holmquist and Vicki Wysocki (OSU) enabled native mass spectrometry samples to assess sample integrity via the Native MS-guided Structural Biology Center funded by NIH RM1GM149374.

References

- [1] S.R. Tzeng, C.G. Kalodimos, Protein dynamics and allostery: An NMR view, Curr. Opin. Struct. Biol. 21 (2011) 62–67. https://doi.org/10.1016/j.sbi.2010.10.007.
- [2] P.S.M. HILL, Sending Signals, Vib. Commun. Anim. 324 (2021) 86–118. https://doi.org/10.2307/j.ctv22jnrn8.7.
- [3] J.P. Changeux, S.J. Edelstein, Allosteric mechanisms of signal transduction, Science 308 (2005) 1424–1428. https://doi.org/10.1126/science.1108595.
- [4] J. Monod, J.P. Changeux, F. Jacob, Allosteric proteins and cellular control systems, J. Mol. Biol. 6 (1963) 306–329. https://doi.org/10.1016/S0022-2836(63)80091-1.
- [5] D.D. Boehr, R. Nussinov, P.E. Wright, The role of dynamic conformational ensembles in biomolecular recognition, Nat. Chem. Biol. 5 (2009) 789–796. https://doi.org/10.1038/nchembio.232.
- [6] J.E. Baenziger, P.J. Corringer, 3D structure and allosteric modulation of the transmembrane domain of pentameric ligand-gated ion channels, Neuropharmacology 60 (2011) 116–125. https://doi.org/10.1016/j.neuropharm.2010.08.007.
- [7] Q. Cui, M. Karplus, Allostery and cooperativity revisited, Protein Sci. 17 (2008) 1295–1307. https://doi.org/10.1110/ps.03259908.

- [8] C.M. Petit, J. Zhang, P.J. Sapienza, E.J. Fuentes, A.L. Lee, Hidden dynamic allostery in a PDZ domain, Proc. Natl. Acad. Sci. U. S. A. 106 (2009) 18249–18254. https://doi.org/10.1073/pnas.0904492106.
- [9] J.G. Harman, Allosteric regulation of the cAMP receptor protein, Biochim. Biophys. Acta-Protein Struct. Mol. Enzymol. 1547 (2001) 1–17. https://doi.org/10.1016/S0167-4838(01)00187-X.
- [10] S.J. Wodak, E. Paci, N. V. Dokholyan, I.N. Berezovsky, A. Horovitz, J. Li, V.J. Hilser, I. Bahar, J. Karanicolas, G. Stock, P. Hamm, R.H. Stote, J. Eberhardt, Y. Chebaro, A. Dejaegere, M. Cecchini, J.P. Changeux, P.G. Bolhuis, J. Vreede, P. Faccioli, S. Orioli, R. Ravasio, L. Yan, C. Brito, M. Wyart, P. Gkeka, I. Rivalta, G. Palermo, J.A. McCammon, J. Panecka-Hofman, R.C. Wade, A. Di Pizio, M.Y. Niv, R. Nussinov, C.J. Tsai, H. Jang, D. Padhorny, D. Kozakov, T. McLeish, Allostery in Its Many Disguises: From Theory to Applications, Structure 27 (2019) 566–578. https://doi.org/10.1016/j.str.2019.01.003.
- [11] M.A. Astore, A.S. Pradhan, E.H. Thiede, S.M. Hanson, Protein dynamics underlying allosteric regulation, Curr. Opin. Struct. Biol. 84 (2024) 102768. https://doi.org/10.1016/j.sbi.2023.102768.
- [12] G. Manley, J.P. Loria, NMR insights into protein allostery, Arch. Biochem. Biophys. 519 (2012) 223–231. https://doi.org/10.1016/j.abb.2011.10.023.
- [13] S. Grutsch, S. Brüschweiler, M. Tollinger, NMR Methods to Study Dynamic Allostery, PLoS Comput. Biol. 12 (2016) 1–20. https://doi.org/10.1371/journal.pcbi.1004620.
- [14] O. Gampp, H. Kadavath, R. Riek, NMR tools to detect protein allostery, Curr. Opin. Struct. Biol. 86 (2024) 102792. https://doi.org/10.1016/j.sbi.2024.102792.
- [15] J.A. Caro, K.W. Harpole, V. Kasinath, J. Lim, J. Granja, K.G. Valentine, K.A. Sharp, A.J. Wand, Entropy in molecular recognition by proteins, Proc. Natl. Acad. Sci. U. S. A. 114 (2017) 6563–6568. https://doi.org/10.1073/pnas.1621154114.
- [16] P. Gollnick, P. Babitzke, Transcription attenuation, Biochim. Biophys. Acta Gene Struct. Expr. 1577 (2002) 240–250. https://doi.org/10.1016/S0167-4781(02)00455-4.
- [17] P. Gollnick, P. Babitzke, A. Antson, C. Yanofsky, Complexity in Regulation of Tryptophan Biosynthesis in Bacillus subtilis, Annu. Rev. Genet. 39 (2005) 47–68. https://doi.org/10.1146/annurev.genet.39.073003.093745.
- [18] A.A. Antson, J. Otridge, A.M. Brzozowski, E.J. Dodson, G.G. Dodson, K.S. Wilson, T.M. Smith, M. Yang, T. Kurecki, P. Gollnick, The structure of trp rna-binding attenuation protein, Nature 374 (1995) 693–700. https://doi.org/10.1038/374693a0.
- [19] A.A. Antson, E.J. Dodson, G. Dodson, R.B. Greaves, X.P. Chen, P. Gollnick, Structure of the trp RNA-binding attenuation protein, TRAP, bound to RNA, Nature 401 (1999) 235– 242. https://doi.org/10.1038/45730.

- [20] A.D. Malay, M. Watanabe, J.G. Heddle, J.R.H. Tame, Crystal structure of unliganded TRAP: Implications for dynamic allostery, Biochem. J. 434 (2011) 427–434. https://doi.org/10.1042/BJ20101813.
- [21] M.L. Holmquist, E.C. Ihms, P. Gollnick, V.H. Wysocki, M.P. Foster, Population Distributions from Native Mass Spectrometry Titrations Reveal Nearest-Neighbor Cooperativity in the Ring-Shaped Oligomeric Protein TRAP, Biochemistry (2020). https://doi.org/10.1021/acs.biochem.0c00352.
- [22] E.C. Ihms, I.R. Kleckner, P. Gollnick, M.P. Foster, Mechanistic Models Fit to Variable Temperature Calorimetric Data Provide Insights into Cooperativity, Biophys. J. 112 (2017) 1328–1338. https://doi.org/10.1016/j.bpj.2017.02.031.
- [23] P. Babitzke, D.G. Bear, C. Yanofsky, TRAP, the trp RNA-binding attenuation protein of Bacillus subtilis, is a toroid-shaped molecule that binds transcripts containing GAG or UAG repeats separated by two nucleotides, Proc. Natl. Acad. Sci. U. S. A. 92 (1995) 7916–7920. https://doi.org/10.1073/pnas.92.17.7916.
- [24] C. McElroy, A. Manfredo, A. Wendt, P. Gollnick, M. Foster, TROSY-NMR studies of the 91 kDa TRAP protein reveal allosteric control of a gene regulatory protein by ligand-altered flexibility, J. Mol. Biol. 323 (2002) 463–473. https://doi.org/10.1016/S0022-2836(02)00940-3.
- [25] I.R. Kleckner, P. Gollnick, M.P. Foster, Mechanisms of allosteric gene regulation by NMR quantification of microsecond-millisecond protein dynamics, J. Mol. Biol. 415 (2012) 372–381. https://doi.org/10.1016/j.jmb.2011.11.019.
- [26] P.F. Flynn, A. Wendt, P. Gollnick, Influence of induced fit in the interaction of Bacillus subtilis trp RNA-binding attenuator protein and its RNA antiterminator target oligomer, Proteins Struct. Funct. Genet. 49 (2002) 432–438. https://doi.org/10.1002/prot.10243.
- [27] B. Reif, S.E. Ashbrook, L. Emsley, M. Hong, Solid-state NMR spectroscopy, Nat. Rev. Methods Primer 1 (2021). https://doi.org/10.1038/s43586-020-00002-1.
- [28] P. Schanda, M. Ernst, Studying dynamics by magic-angle spinning solid-state NMR spectroscopy: Principles and applications to biomolecules, Prog. Nucl. Magn. Reson. Spectrosc. 96 (2016) 1–46. https://doi.org/10.1016/j.pnmrs.2016.02.001.
- [29] A.B. Siemer, Advances in studying protein disorder with solid-state NMR, Solid State Nucl. Magn. Reson. 106 (2020) 101643. https://doi.org/10.1016/j.ssnmr.2020.101643.
- [30] C.P. Jaroniec, Two decades of progress in structural and dynamic studies of amyloids by solid-state NMR, J. Magn. Reson. 306 (2019) 42–47. https://doi.org/10.1016/j.jmr.2019.07.015.
- [31] A. Loquet, B. Habenstein, A. Lange, by Solid-State NMR, Acc. Chemi 46 (2013).

- [32] G. Porat-Dahlerbruch, A. Goldbourt, T. Polenova, Virus Structures and Dynamics by Magic-Angle Spinning NMR, Annu. Rev. Virol. 8 (2021) 219–237. https://doi.org/10.1146/annurev-virology-011921-064653.
- [33] B.E. Ackermann, G.T. Debelouchina, Emerging Contributions of Solid-State NMR Spectroscopy to Chromatin Structural Biology, Front. Mol. Biosci. 8 (2021) 1–12. https://doi.org/10.3389/fmolb.2021.741581.
- [34] S.D. Gorman, D. Sahu, K.F. O'Rourke, D.D. Boehr, Assigning methyl resonances for protein solution-state NMR studies, Methods 148 (2018) 88–99. https://doi.org/10.1016/j.ymeth.2018.06.010.
- [35] X.P. Chen, A.A. Antson, M.Y.P. Li, C. Baumann, E.J. Dodson, G.G. Dodson, P. Gollnick, Erratum: Regulatory features of the trp operon and the crystal structure of the trp RNAbinding attenuation protein from Bacillus stearothermophilus (Journal of Molecular Biology (1999) 289, (1003-1016)), J. Mol. Biol. 291 (1999) 727. https://doi.org/10.1006/jmbi.1999.3050.
- [36] A.G. Palmer, H. Koss, Chemical Exchange, 1st ed., Elsevier Inc., 2019. https://doi.org/10.1016/bs.mie.2018.09.028.
- [37] I.R. Kleckner, M.P. Foster, An introduction to NMR-based approaches for measuring protein dynamics, Biochim. Biophys. Acta BBA Proteins Proteomics 1814 (2011) 942–968. https://doi.org/10.1016/j.bbapap.2010.10.012.
- [38] R. Ishima, D.A. Torchia, Estimating the time scale of chemical exchange of proteins from measurements of transverse relaxation rates in solution, J. Biomol. NMR 14 (1999) 369–372. https://doi.org/10.1023/A:1008324025406.
- [39] O. Millet, J.P. Loria, C.D. Kroenke, M. Pons, A.G. Palmer, The static magnetic field dependence of chemical exchange linebroadening defines the NMR chemical shift time scale, J. Am. Chem. Soc. 122 (2000) 2867–2877. https://doi.org/10.1021/ja993511y.
- [40] D.M. LeMaster, NMR relaxation order parameter analysis of the dynamics of protein side chains, J. Am. Chem. Soc. 121 (1999) 1726–1742. https://doi.org/10.1021/ja982988r.
- [41] N. Müller, G. Bodenhausen, R.R. Ernst, Relaxation-induced violations of coherence transfer selection rules in nuclear magnetic resonance, J. Magn. Reson. 1969 75 (1987) 297–334. https://doi.org/10.1016/0022-2364(87)90038-2.
- [42] V. Tugarinov, R. Sprangers, L.E. Kay, Probing side-chain dynamics in the proteasome by relaxation violated coherence transfer NMR spectroscopy, J. Am. Chem. Soc. 129 (2007) 1743–1750. https://doi.org/10.1021/ja067827z.
- [43] G. Lipari, A. Szabo, Model-Free Approach to the Interpretation of Nuclear Magnetic Resonance Relaxation in Macromolecules. 2. Analysis of Experimental Results, J. Am. Chem. Soc. 104 (1982) 4559–4570. https://doi.org/10.1021/ja00381a010.

- [44] V.A. Higman, Solid-state MAS NMR resonance assignment methods for proteins, Prog. Nucl. Magn. Reson. Spectrosc. 106–107 (2018) 37–65. https://doi.org/10.1016/j.pnmrs.2018.04.002.
- [45] Y. Shen, A. Bax, Protein backbone and sidechain torsion angles predicted from NMR chemical shifts using artificial neural networks, J. Biomol. NMR 56 (2013) 227–241. https://doi.org/10.1007/s10858-013-9741-y.
- [46] K. Aebischer, M. Ernst, INEPT and CP transfer efficiencies of dynamic systems in MAS solid-state NMR, J. Magn. Reson. 359 (2024) 107617. https://doi.org/10.1016/j.jmr.2024.107617.
- [47] I. Matlahov, P.C.A. van der Wel, Hidden motions and motion-induced invisibility: Dynamics-based spectral editing in solid-state NMR, Methods 148 (2018) 123–135. https://doi.org/10.1016/j.ymeth.2018.04.015.
- [48] J.J. Helmus, K. Surewicz, W.K. Surewicz, C.P. Jaroniec, Conformational flexibility of Y145stop human prion protein amyloid fibrils probed by solid-state nuclear magnetic resonance spectroscopy, J. Am. Chem. Soc. 132 (2010) 2393–2403. https://doi.org/10.1021/ja909827v.
- [49] G. Cornilescu, A. Bax, D.A. Case, Large variations in one-bond 13C(α)13C(β) J couplings in polypeptides correlate with backbone conformation, J. Am. Chem. Soc. 122 (2000) 2168–2171. https://doi.org/10.1021/ja993609c.
- [50] V.A. Higman, Solid-state MAS NMR resonance assignment methods for proteins, Prog. Nucl. Magn. Reson. Spectrosc. 106–107 (2018) 37–65. https://doi.org/10.1016/j.pnmrs.2018.04.002.
- [51] L. Siemons, B. Uluca-Yazgi, R.B. Pritchard, S. McCarthy, H. Heise, D.F. Hansen, Determining isoleucine side-chain rotamer-sampling in proteins from 13C chemical shift, Chem. Commun. 55 (2019) 14107–14110. https://doi.org/10.1039/c9cc06496f.
- [52] D.F. Hansen, P. Neudecker, L.E. Kay, Determination of isoleucine side-chain conformations in ground and excited states of proteins from chemical shifts, J. Am. Chem. Soc. 132 (2010) 7589–7591. https://doi.org/10.1021/ja102090z.
- [53] S.C. Lovell, J.M. Word, J.S. Richardson, D.C. Richardson, The penultimate rotamer library, Proteins Struct. Funct. Bioinforma. 40 (2000) 389–408. https://doi.org/10.1002/1097-0134(20000815)40:3<389::AID-PROT50>3.0.CO;2-2.
- [54] I.R. Kleckner, C.A. McElroy, P. Kuzmic, P. Gollnick, M.P. Foster, Homotropic cooperativity from the activation pathway of the allosteric ligand-responsive regulatory trp RNA-binding attenuation protein, Biochemistry 52 (2013) 8855–8865. https://doi.org/10.1021/bi401364v.
- [55] N.M. Mcadams, A. Patterson, P. Gollnick, crossm Identification of a Residue (Glu60) in Transcription Termination at the trp, 199 (2017) 1–17.

- [56] N.H. Hopcroft, A.L. Wendt, P. Gollnick, A.A. Antson, Specificity of TRAP-RNA interactions: crystal structures of two complexes with different RNA sequences., Acta Crystallogr. D Biol. Crystallogr. 58 (2002) 615–621. https://doi.org/10.1107/s0907444902003189.
- [57] M.H. Levitt, D. Suter, R.R. Ernst, Spin dynamics and thermodynamics in solid-state NMR cross polarization, J. Chem. Phys. 84 (1986) 4243–4255. https://doi.org/10.1063/1.450046.
- [58] M. Baldus, A.T. Petkova, J. Herzfeld, R.G. Griffin, Cross polarization in the tilted frame: Assignment and spectral simplification in heteronuclear spin systems, Mol. Phys. 95 (1998) 1197–1207. https://doi.org/10.1080/00268979809483251.
- [59] C.A. Smith, D. Ban, S. Pratihar, K. Giller, C. Schwiegk, B.L. de Groot, S. Becker, C. Griesinger, D. Lee, Population Shuffling of Protein Conformations, Angew. Chem. Int. Ed. 54 (2015) 207–210. https://doi.org/10.1002/anie.201408890.
- [60] J.J. Chou, D.A. Case, A. Bax, Insights into the Mobility of Methyl-Bearing Side Chains in Proteins from 3JCC and 3JCN Couplings, J. Am. Chem. Soc. 125 (2003) 8959–8966. https://doi.org/10.1021/ja029972s.
- [61] P. Schanda, M. Huber, J. Boisbouvier, B.H. Meier, M. Ernst, Solid-State NMR Measurements of Asymmetric Dipolar Couplings Provide Insight into Protein Side-Chain Motion, Angew. Chem. Int. Ed. 50 (2011) 11005–11009. https://doi.org/10.1002/anie.201103944.
- [62] B.S. Ibrahim, V. Pattabhi, Role of weak interactions in thermal stability of proteins, Biochem. Biophys. Res. Commun. 325 (2004) 1082–1089. https://doi.org/10.1016/j.bbrc.2004.10.128.
- [63] R.W. Harkness, Y. Toyama, L.E. Kay, Analyzing multi-step ligand binding reactions for oligomeric proteins by NMR: Theoretical and computational considerations, J. Magn. Reson. 318 (2020) 106802. https://doi.org/10.1016/j.jmr.2020.106802.
- [64] W. Li, A.S. Norris, K. Lichtenthal, S. Kelly, E.C. Ihms, P. Gollnick, V.H. Wysocki, M.P. Foster, Thermodynamic coupling between neighboring binding sites in homo-oligomeric ligand sensing proteins from mass resolved ligand-dependent population distributions, Protein Sci. Publ. Protein Soc. 31 (2022) e4424. https://doi.org/10.1002/pro.4424.
- [65] M.R. Eftink, A.C. Anusiem, R.L. Biltonen, Enthalpy-entropy compensation and heat capacity changes for protein-ligand interactions: general thermodynamic models and data for the binding of nucleotides to ribonuclease A, Biochemistry 22 (1983) 3884–96.
- [66] N.V. Prabhu, K.A. Sharp, Heat Capacity in Proteins, Annu. Rev. Phys. Chem. 56 (2005) 521–548. https://doi.org/10.1146/annurev.physchem.56.092503.141202.
- [67] Y. Wang, M. V.S, J. Kim, G. Li, L.G. Ahuja, P. Aoto, S.S. Taylor, G. Veglia, Globally correlated conformational entropy underlies positive and negative cooperativity in a

- kinase's enzymatic cycle, Nat. Commun. 10 (2019). https://doi.org/10.1038/s41467-019-08655-7.
- [68] D.A. Capdevila, J.J. Braymer, K.A. Edmonds, H. Wu, D.P. Giedroc, Entropy redistribution controls allostery in a metalloregulatory protein, Proc. Natl. Acad. Sci. U. S. A. 114 (2017) 4424–4429. https://doi.org/10.1073/pnas.1620665114.
- [69] K.K. Frederick, M.S. Marlow, K.G. Valentine, A.J. Wand, Conformational entropy in molecular recognition by proteins, Nature 448 (2007) 325–329. https://doi.org/10.1038/nature05959.
- [70] M.S. Marlow, J. Dogan, K.K. Frederick, K.G. Valentine, A.J. Wand, The role of conformational entropy in molecular recognition by calmodulin, Nat. Chem. Biol. 6 (2010) 352–358. https://doi.org/10.1038/nchembio.347.
- [71] T.I. Igumenova, K.K. Frederick, A.J. Wand, Characterization of the Fast Dynamics of Protein Amino Acid Side Chains Using NMR Relaxation in Solution, (2006) 1672–1699.
- [72] R.S. Spolar, M.T. Record Jr., Coupling of local folding to site-specific binding of proteins to DNA, Science 263 (1994) 777–84.
- [73] D. Yang, L.E. Kay, Contributions to conformational entropy arising from bond vector fluctuations measured from NMR-derived order parameters: Application to protein folding, J. Mol. Biol. 263 (1996) 369–382. https://doi.org/10.1006/jmbi.1996.0581.
- [74] F. Delaglio, S. Grzesiek, G.W. Vuister, G. Zhu, J. Pfeifer, A. Bax, NMRPipe: A multidimensional spectral processing system based on UNIX pipes, J. Biomol. NMR 6 (1995) 277–293. https://doi.org/10.1007/BF00197809.
- [75] I.R. Kleckner, M.P. Foster, GUARDD: User-friendly MATLAB software for rigorous analysis of CPMG RD NMR data, J. Biomol. NMR 52 (2012) 11–22. https://doi.org/10.1007/s10858-011-9589-y.
- [76] C.A. McElroy, DYNAMICS AND FUNCTION: MECHANISTIC STUDIES OF THE GENE REGULATORY PROTEINS TRAP AND ANTI-TRAP, (2005) 1–343.
- [77] F. Zhang, R. Brüschweiler, Contact model for the prediction of NMR N-H order parameters in globular proteins, J. Am. Chem. Soc. 124 (2002) 12654–12655. https://doi.org/10.1021/ja027847a.
- [78] D. Ming, R. Brüschweiler, Prediction of methyl-side Chain Dynamics in Proteins, J. Biomol. NMR 29 (2004) 363–368. https://doi.org/10.1023/B:JNMR.0000032612.70767.35.
- [79] B.M. Fung, A.K. Khitrin, K. Ermolaev, An Improved Broadband Decoupling Sequence for Liquid Crystals and Solids, J. Magn. Reson. 142 (2000) 97–101. https://doi.org/10.1006/jmre.1999.1896.

Journal Pre-proofs

- [80] K. Takegoshi, S. Nakamura, T. Terao, 13C-1H dipolar-driven 13C-13C recoupling without 13C rf irradiation in nuclear magnetic resonance of rotating solids, J. Chem. Phys. 118 (2003) 2325–2341. https://doi.org/10.1063/1.1534105.
- [81] J. Hoffmann, J. Ruta, C. Shi, K. Hendriks, V. Chevelkov, W.T. Franks, H. Oschkinat, K. Giller, S. Becker, A. Lange, Protein resonance assignment by BSH-CP-based 3D solid-state NMR experiments: A practical guide, Magn. Reson. Chem. 58 (2020) 445–465. https://doi.org/10.1002/mrc.4945.
- [82] M. Baldus, A.T. Petkova, J. Herzfeld, R.G. Griffin, Cross polarization in the tilted frame: Assignment and spectral simplification in heteronuclear spin systems, Mol. Phys. 95 (1998) 1197–1207. https://doi.org/10.1080/00268979809483251.
- [83] L. Chen, R.A. Olsen, D.W. Elliott, J.M. Boettcher, D.H. Zhou, C.M. Rienstra, L.J. Mueller, Constant-time through-bond 13C correlation spectroscopy for assigning protein resonances with solid-state NMR spectroscopy, J. Am. Chem. Soc. 128 (2006) 9992–9993. https://doi.org/10.1021/ja062347t.

Supplemental

Insights into Ligand-Mediated Activation of an Oligomeric Ring-Shaped Gene-Regulatory Protein from Solution and Solid-State NMR

Rodrigo Muzquiz^{a,b}, Cameron Jamshidi^{a,b}, Daniel W. Conroy^b, Christopher P. Jaroniec^{a,b}, and Mark P. Foster^{a,b,*}

^a Ohio State Biochemistry Graduate Program, The Ohio State University, 484 West 12th Avenue, Columbus, OH 43210, USA

^b Department of Chemistry and Biochemistry, The Ohio State University, 100 West 18th Avenue, Columbus, OH 43210, USA

*Correspondence to: foster.281@osu.edu; 614-292-1377

From	То	Distance (Å)	HCH Cross-Peak	CCH Cross-Peak	Notes
lle61	Thr63	7.4	Yes	Yes	
lle43	Thr63	4.8	Yes	Yes	
Thr63	lle61	7.4	Yes	Yes	
lle53	Thr50	4.5	Yes	Yes	
Thr50	lle53	4.5	Yes	Yes	
lle20	Thr28	11.2	No	Yes	
lle26	Thr23	6.9	Yes	Yes	*No crystal structure of mutation
Thr23	lle26	6.9	Yes	Yes	*No crystal structure of mutation
Thr28	lle20	11.2	Yes	No	
Thr50	Thr47	5.7	No	Yes	

Table S 1. Methyl-Methyl NOESY Cross peak assignment table.

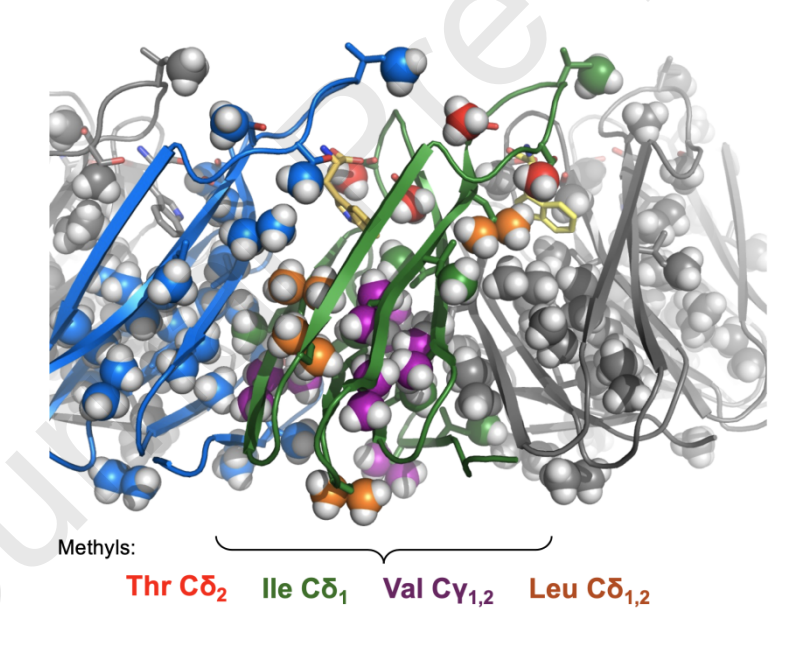


Figure S 1. Location of methyl probes in undecameric Gst TRAP protomers. The backbone cartoons of three chains are blue, green, grey, respectively, and Ala, Ile, Leu and Val methyl groups are shown as spheres. In the green protomer, methyl groups carbons that have been labeled for NMR studies are colored by residue type: Thr $C\gamma_2$ red, Ile $C\delta_1$ green, Val $C\gamma_{1,2}$ purple, and Leu $C\delta_{1,2}$ orange. In the present study, Thr and Ile methyl groups are labeled. Val and Leu methyls were also labeled in previous studies [25]. The coordinates used are IC9S with Ala26 replaced with Ile using PyMOL.

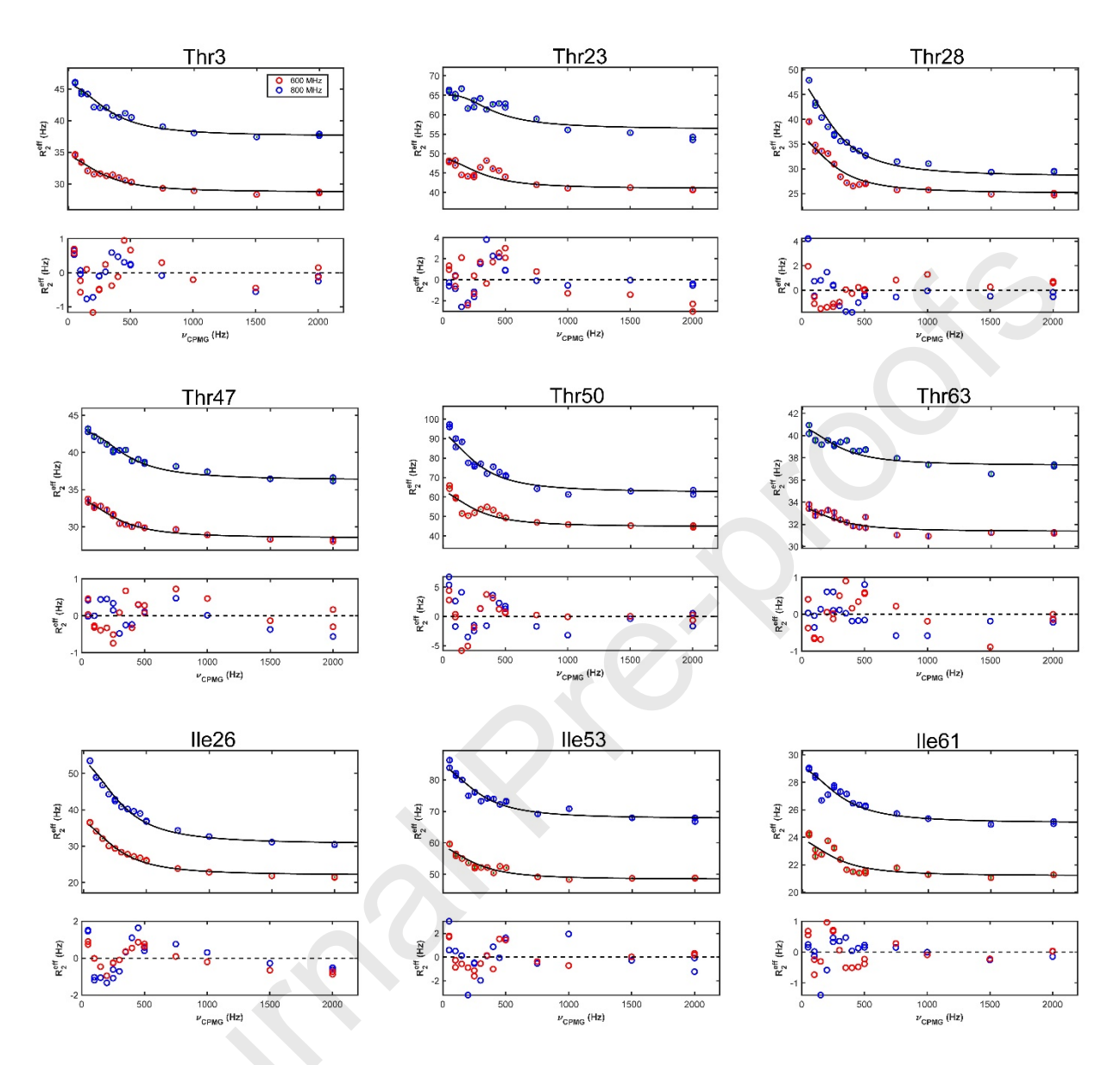


Figure S 2: Globally fit methyl RD curves of apo-A26I-TRAP at 20°C at 600 (red) and 800 (blue) MHz B_0 field strength. The RD curves for all six threonine and three of the Ile $\delta 1$ methyl groups (Ile26, Ile53, Ile61) could be globally fit to a single two-state exchange process with a $k_{\rm ex}$ value of $1700 \pm 300~{\rm s}^{-1}$.

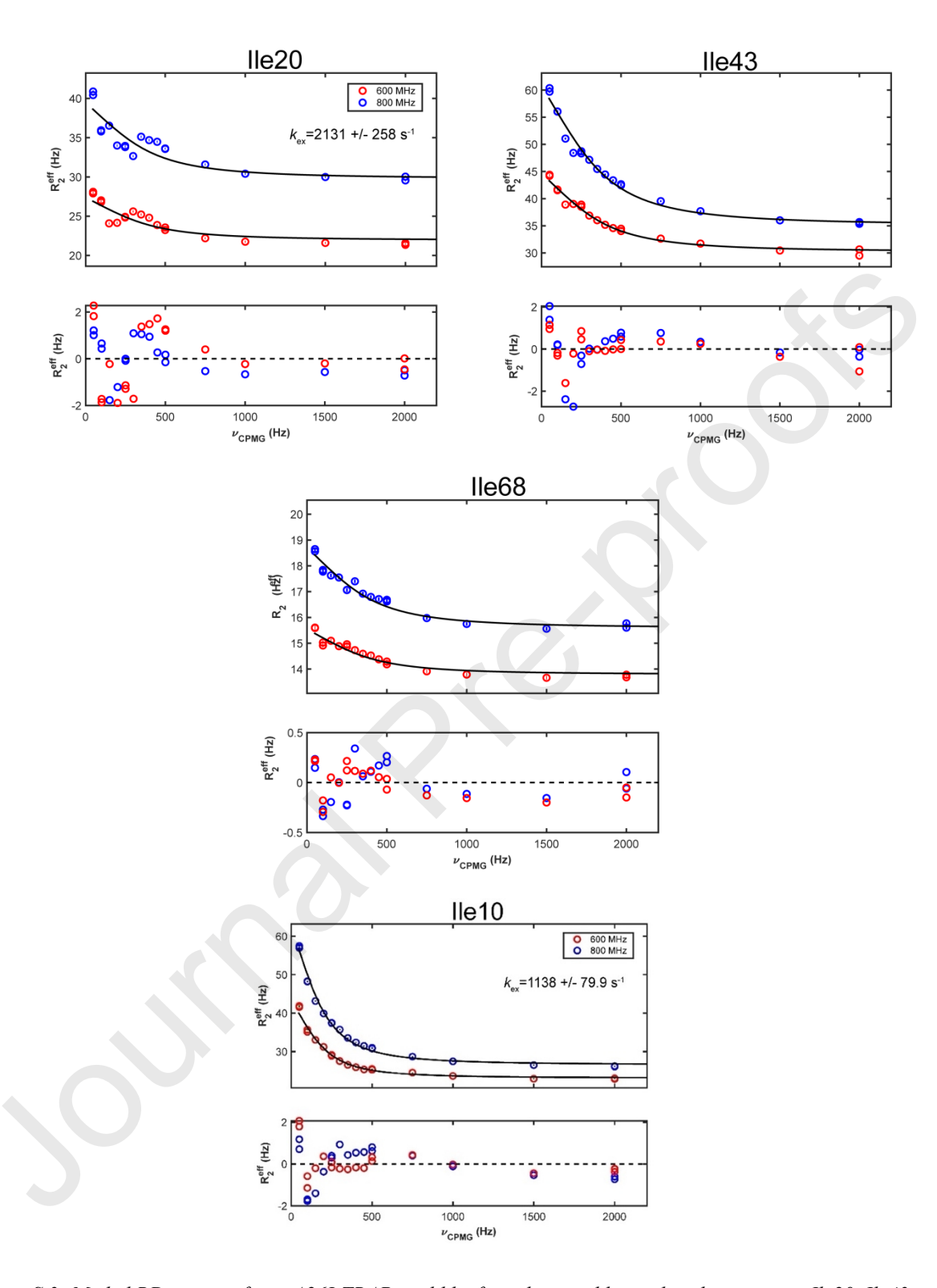


Figure S 3: Methyl RD curves of apo-A26I-TRAP could be fit with two additional exchange rates. Ile20, Ile43 and Il68, each in the inter-protomer interface can be globally fit with a two-state model with a $k_{ex} = 2100 \pm 300 \text{ s}^{-1}$, while fitting of the Ile10 methyl RD curves is best described by a exchange rate of $1140 \pm 80 \text{ s}^{-1}$. Individual and global fits of RD curves were performed using GUARDD [75].

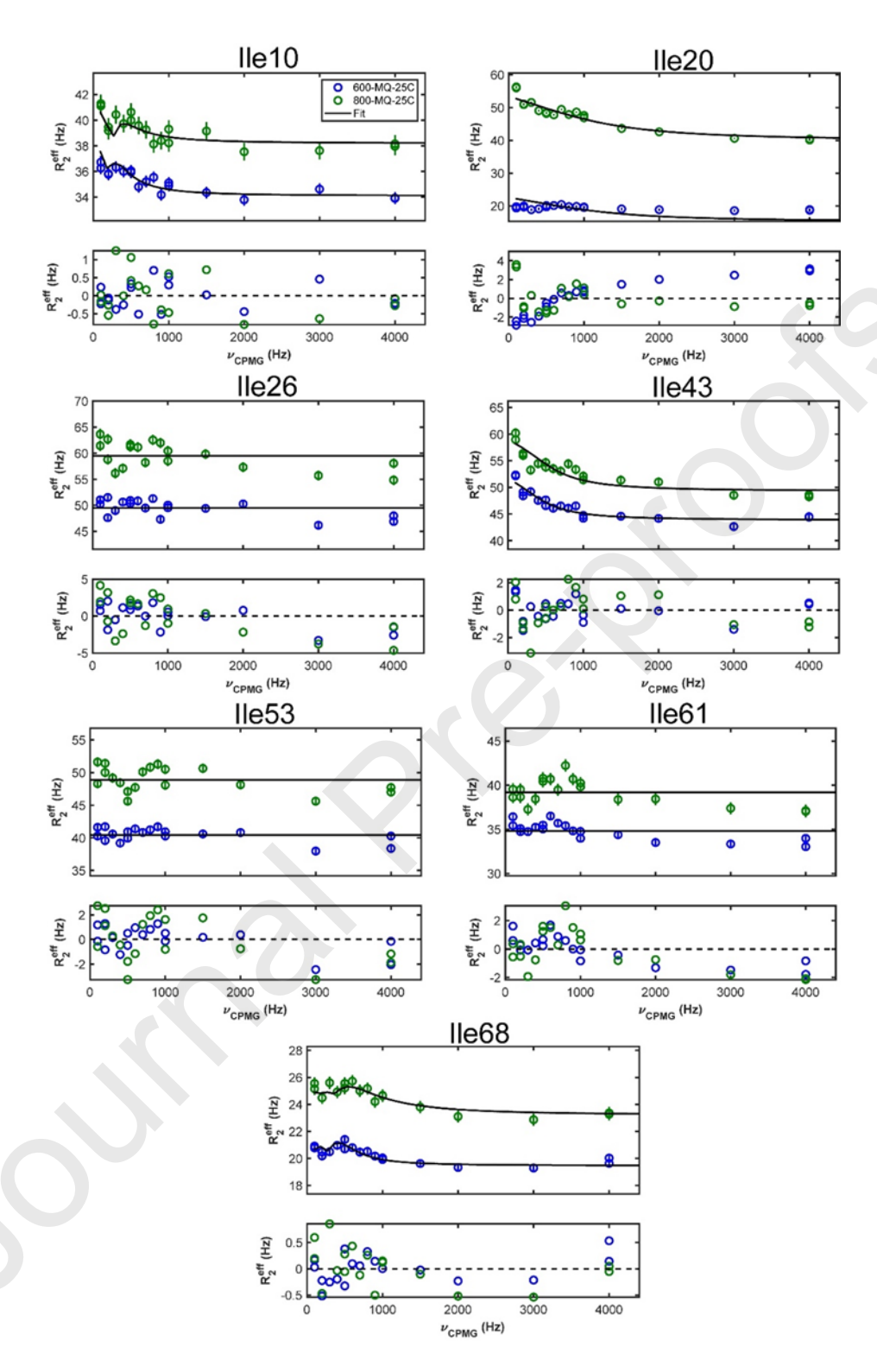


Figure S 4: Methyl RD curves of holo-A26I TRAP collected at 20°C and field strengths of 600 and 800 MHz. Ile residues 26, 53, and 61 show no dispersions in Trp-bound TRAP, while the methyl groups of several Ile residues retain relaxation dispersion profiles: Ile10 ($280 \pm 50 \text{ s}^{-1}$), Ile20 ($7600 \pm 1700 \text{ s}^{-1}$), 43 ($2200 \pm 600 \text{ s}^{-1}$) and 68 ($1600 \pm 400 \text{ s}^{-1}$). Global fitting of these provides resulted in poor fits, so only individual fits are reported.

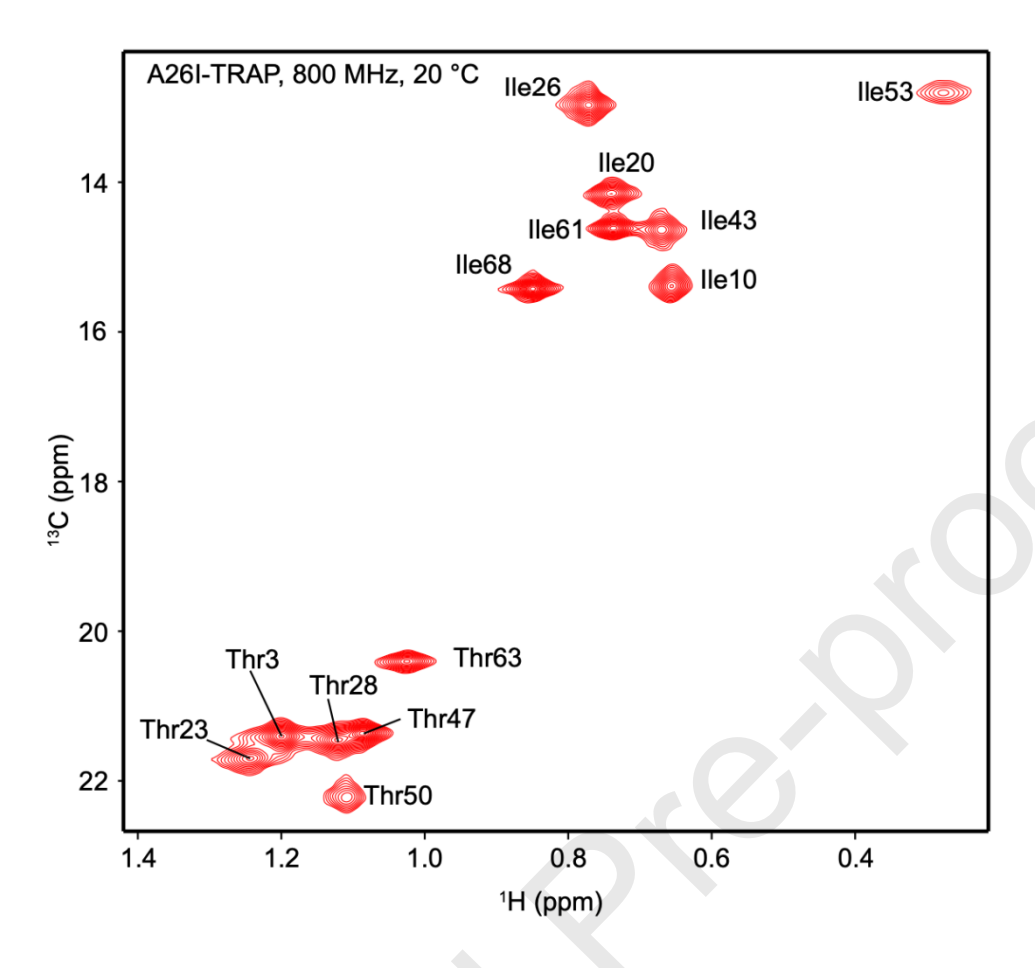


Figure S 5: TROSY-HMQC of apo $[U^2H]^{15}N$, Ile/Thr-methyl ^{13}C]-A26I-TRAP at 800 MHz, 20 °C. Representative spectrum corresponding to conditions for methyl CPMG relaxation dispersion experiments.

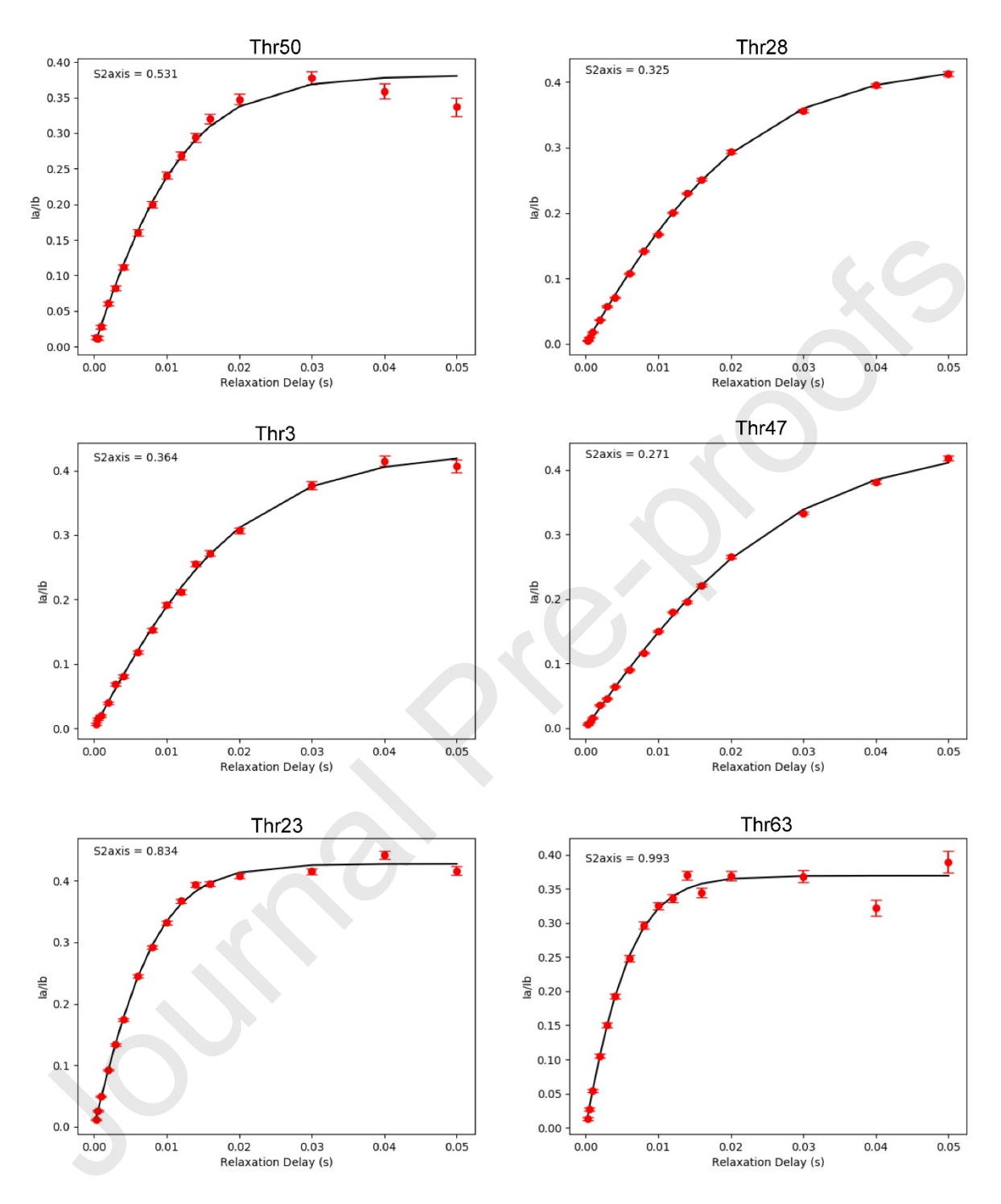


Figure S 6: γ₂ Methyl DQC/SQC buildup Curves for Thr residues in apo A26I TRAP.

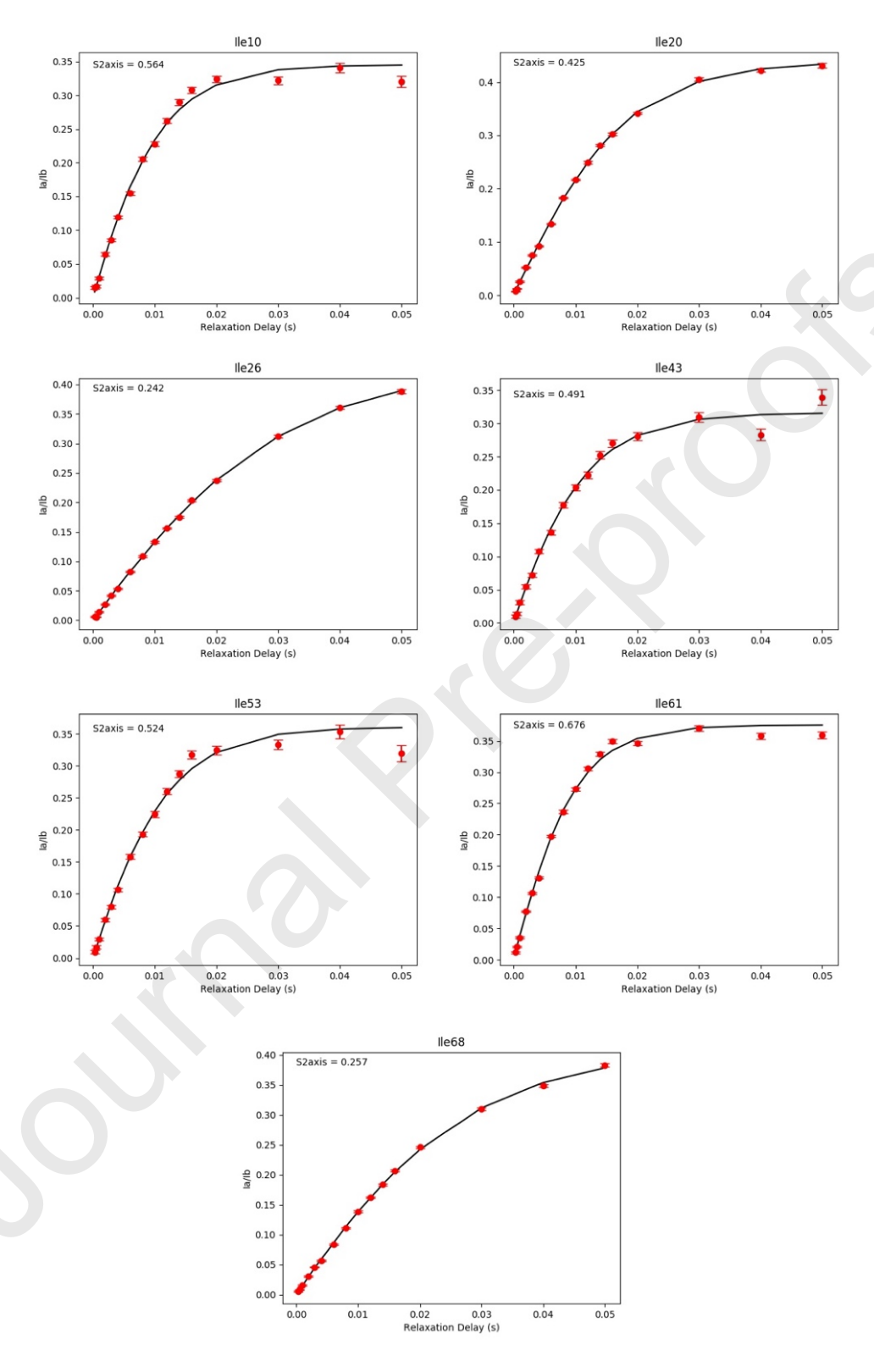


Figure S 7: δ_1 Methyl DQC/SQC buildup Curves for Ile residues in apo A26I TRAP.

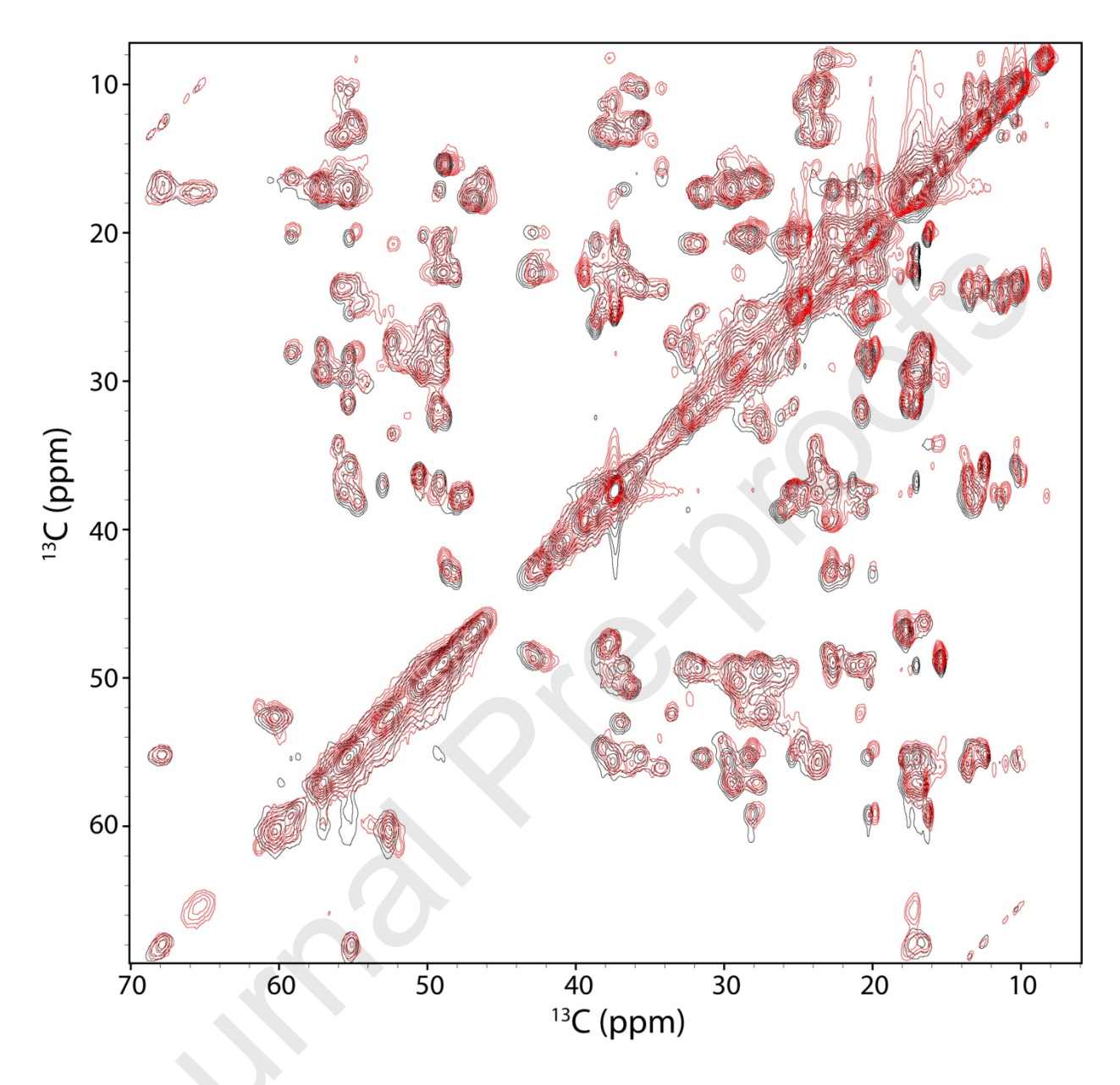


Figure S 8: Solid-state CP spectra of apo TRAP is not strongly sensitive to temperature. Fingerprint region of the ^{13}C - ^{13}C DARR chemical shift correlation spectra of apo TRAP at 4°C (black) and ~45°C (red) using a mixing time of 15 ms at 11.111 kHz MAS speed in a 3.2 mm rotor at 800 MHz.

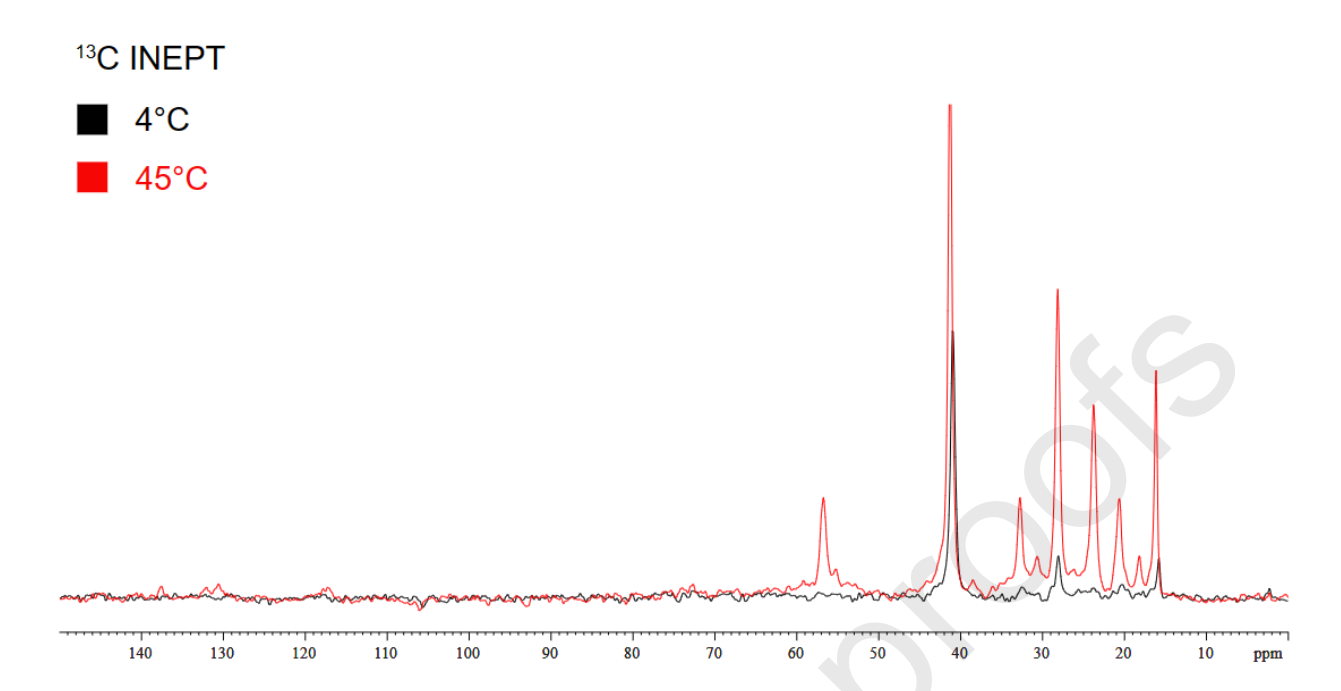


Figure S 9: $1D^{13}C$ INEPT spectra of WT apo TRAP at 800 MHz field strength, under a MAS speed of 11.111 kHz in a 3.2 mm rotor at high and low temperatures shows an increase in signal.

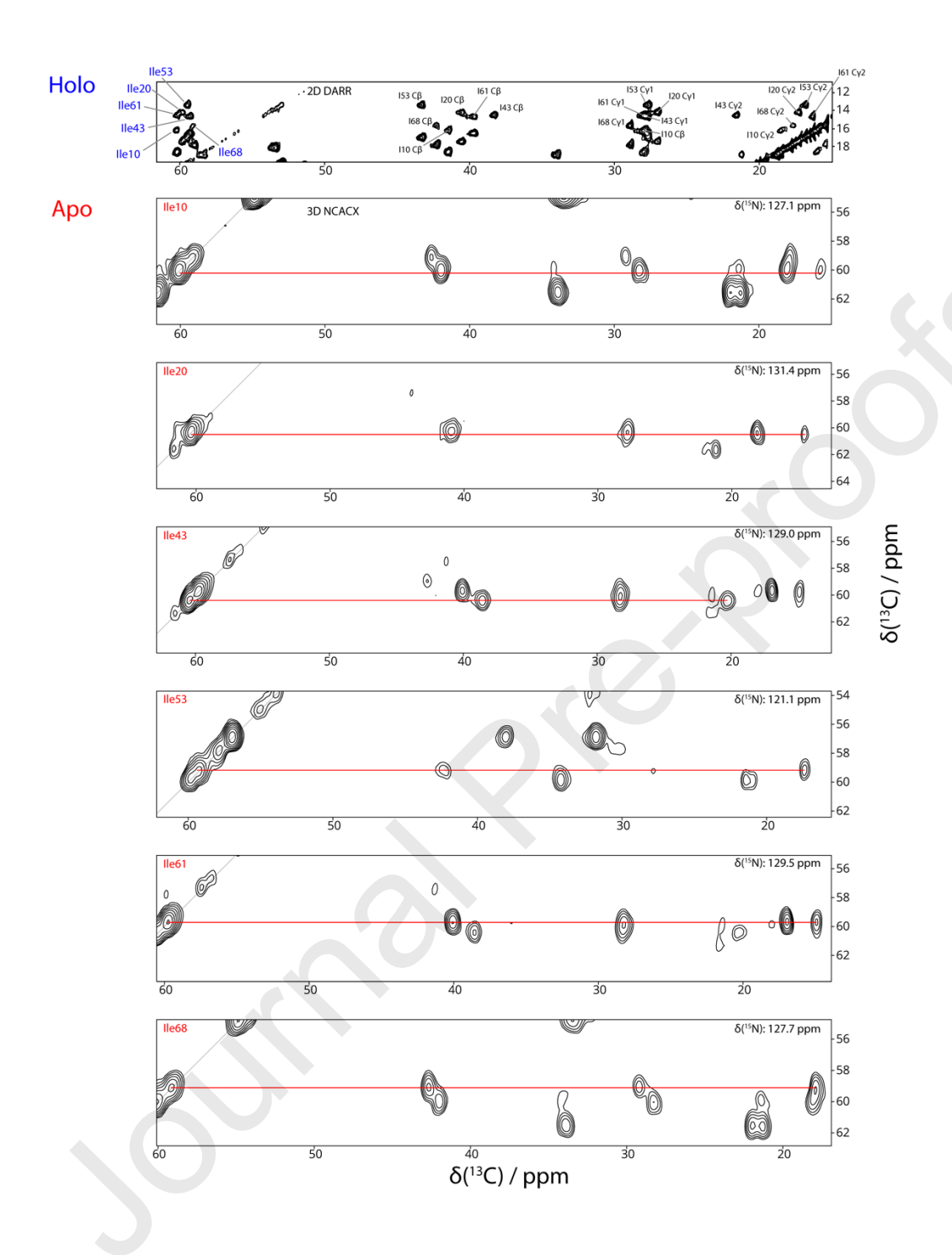


Figure S 10:Top, ¹³C DARR of holo Trp-TRAP recorded with 15 ms mixing time on a 1.2 GHz instrument at 4 °C MAS: 12 kHz. Correlations are observed along the entire side chain, allowing direct ¹³C assignments for all Ile in the protein. (For the WT protein residue 26 is Ala, not Ile.) Bottom, strips from the 3D NCACX spectrum of apo TRAP, recorded at 800 MHz, illustrating assignments of the Ile ¹³C resonances in apo TRAP. Comparison of the sidechain ¹³C shifts in these spectra reveal changes in rotamer distributions.

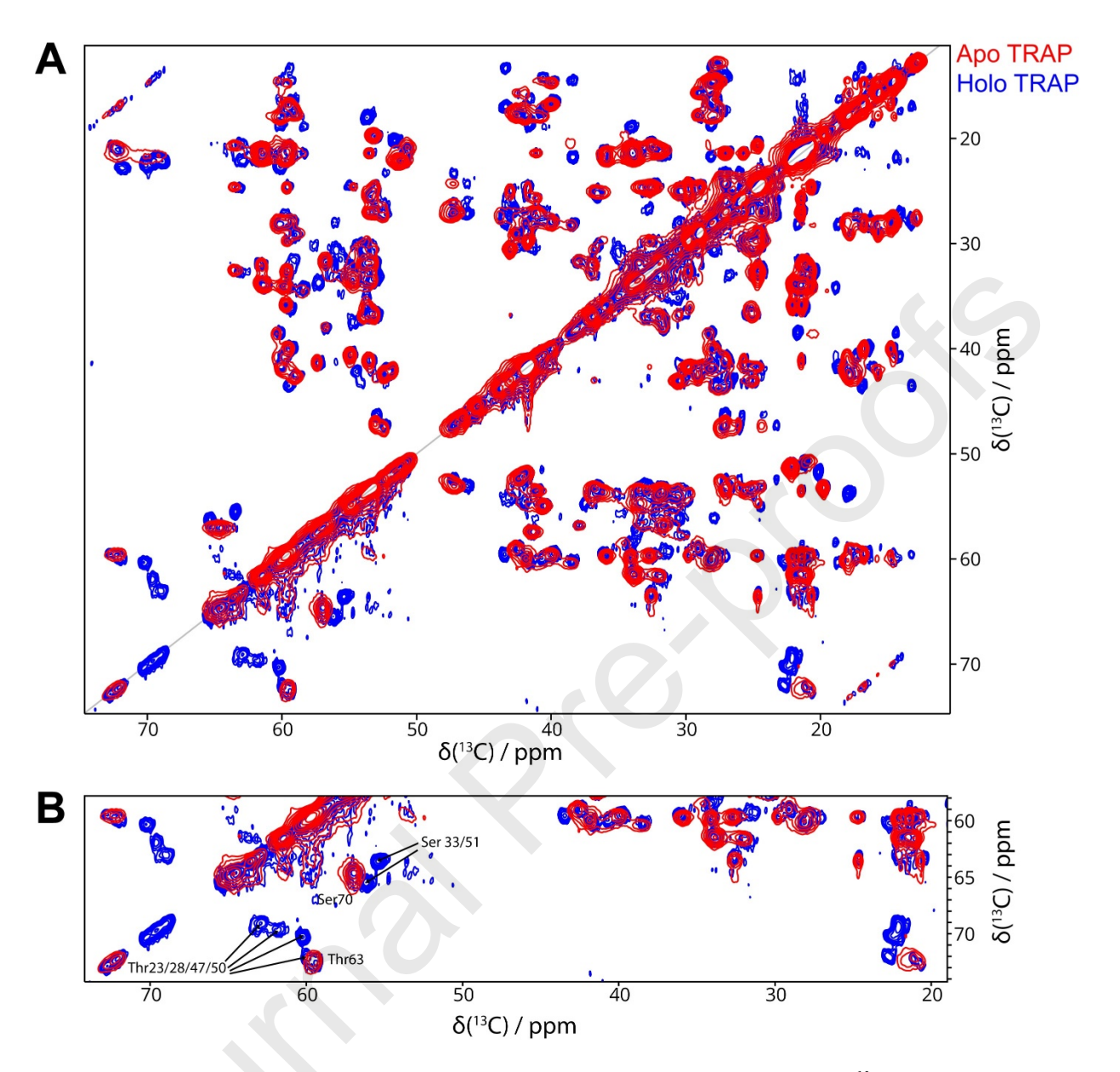


Figure S 11: CP-based MAS NMR spectra reveal increased order in Trp-bound TRAP. A, 13 C DARR of apo TRAP (red) and holo TRAP (blue) recorded on an 800 MHz instrument at 4°C MAS: 11 kHz with a mixing time of 15 ms. Trp-bound TRAP features additional resonances in 13 C correlation spectra narrower signals. B, Expanded view of Thr Ca shift region shows rigidification of Thr residues as evidenced by the appearance of four new sets of Ca/C β correlations not observed in the spectrum of apo TRAP.

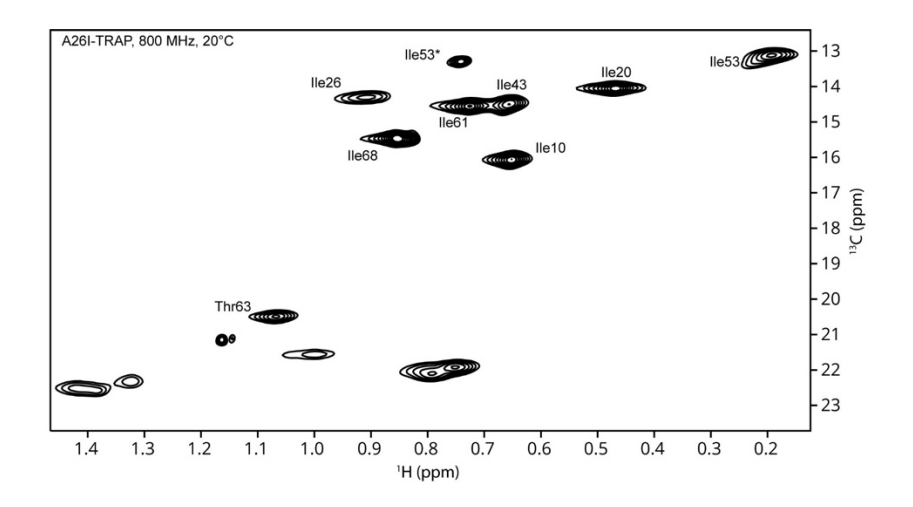


Figure S 12: Methyl TROSY HMQC of holo A26I-TRAP at 800 MHz and 20°C.

Calculation of Entropy from Order Parameters

We calculated the change in conformational entropy from the methyl order parameters using the previously described relationship [73].

$$\frac{\Delta S_p(j)}{k} = \ln \left\{ [3 - (1 + 8 * S_b)^{\frac{1}{2}}] / [3 - (1 + 8 * S_a)^{\frac{1}{2}}] \right\}$$

Where S_b and S_a are the order parameters of the methyl bond in states b and a respectively and $S_p(j)$ is the total rotational entropy change for the methyl bond j. This model assumes that motion occurs as diffusion-in-a-cone. Under the assumption that state changes from a to b occur as concerted motion amongst all Thr/Ile methyl probes, the average ΔS_p was used to calculate the entropic contributions to free energy (ΔS_{conf}) using the following equation.

$$\Delta S_{conf} = \frac{\Delta S_p(j)}{k} * \frac{N}{k} * 4.18 * T$$

Where k is the Boltzmann constant, N is Avogadro's number, and T is temperature in kelvin, providing the energy in keal mol⁻¹.

Journal Pre-proofs

Insights into Ligand-Mediated Activation of an Oligomeric Ring-Shaped Gene-Regulatory Protein

from Solution- and Solid-State NMR

Rodrigo Muzquiz^{a,b}, Cameron Jamshidi^{a,b}, Daniel W. Conroy^b, Christopher P. Jaroniec^{a,b}, and Mark P. Foster^{a,b,*}

^a Ohio State Biochemistry Graduate Program, The Ohio State University, 484 West 12th Avenue, Columbus, OH 43210, USA

^b Department of Chemistry and Biochemistry, The Ohio State University, 100 West 18th Avenue, Columbus, OH 43210, USA

*Correspondence to: foster.281@osu.edu; 614-292-1377

Declarations of interest: none